

UC Berkeley

UC Berkeley Electronic Theses and Dissertations

Title

Lateral Diffusion of GABAARs Studied with a Novel Electrophysiological Technique: CREAP

Permalink

<https://escholarship.org/uc/item/3r92h6c7>

Author

Smith, Caleb Morgan

Publication Date

2018

Peer reviewed|Thesis/dissertation

**Lateral Diffusion of GABA_ARs Studied with a Novel Electrophysiological Technique:
CREAP**

By
Caleb Smith

A dissertation submitted in partial satisfaction of the
requirements for the degree of
Doctor of Philosophy
In
Molecular and Cell Biology
In the
Graduate Division
Of the
University of California, Berkeley

Committee in charge:
Professor Richard Kramer, Chair
Professor Hillel Adesnik
Professor Dan Feldman
Professor Frederick Theunissen

Spring 2018

**Lateral Diffusion of GABA_ARs Studied with a Novel Electrophysiological Technique:
CREAP**

© 2018

By Caleb Smith

Abstract

Lateral Diffusion of GABA_ARs Studied with a Novel Electrophysiological Technique: CREAP

By Caleb Smith

Doctor of Philosophy in Molecular and Cell Biology

University of California, Berkeley

Professor Richard Kramer, Chair

GABA_A receptors (GABA_ARs) mediate fast synaptic inhibition in the mammalian brain and are essential for balancing excitation and sharpening our sensory perceptions. GABA_ARs are plastic and respond to changes in neuronal activity by strengthening or weakening inhibitory neurotransmission. This inhibitory plasticity responds to many of the same signals that mediate glutamatergic excitatory plasticity and works in tandem with or in contraposition to excitation to form the cellular basis of memories. GABA_ARs are added to or dispersed from synapses to modulate synaptic strength, and this is achieved by lateral diffusion in the plane of the membrane. By tethering GABA_ARs with synaptic scaffold proteins, primarily gephyrin, the inhibitory synapse can accumulate GABA_ARs dependent on the potency of this interaction. The scaffolds themselves are highly plastic and can agglomerate or wash away in coordination with GABA_ARs. An additional element of this process is the availability of extrasynaptic GABA_ARs able to diffuse into synapses, a supply that is tightly controlled by endo- and exocytosis of receptors from internal endosomal reservoirs and which is important for both acute plasticity and long-term homeostasis. The result is inhibitory synapses that are able to respond to activity changes with structural rearrangements on the scale of minutes to days.

Thus far, GABA_AR mobility has been primarily interrogated with single particle tracking of quantum dots and FRAP in the context of neuronal cultures, where dendrite morphology and molecular composition have been radically altered from *in vivo* conditions. The rise of new optogenetic techniques, which provide great spatial and temporal precision, affords an opportunity to study mobility in more natural and intact conditions such as the acute slice preparation. Here we extend the optogenetic strategy to GABA_ARs, creating a light-regulated GABA_AR (LiGABAR) by conjugating a photo-switchable tethered ligand (PTL) onto a mutant receptor containing a cysteine-substituted $\alpha 1$ -subunit. The installed PTL can be advanced to or retracted from the GABA-binding pocket with 500-nm and 380-nm light, respectively, resulting in photo-switchable receptor antagonism. We created a transgenic knock-in $\alpha 1$ photoswitch-ready mouse ($\alpha 1$ PhoRM) to express the mutant receptor at endogenous levels and distributions.

We make use of LiGABAR technology to pioneer a novel electrophysiological technique for measuring GABA_AR mobility, which we call CREAP. We use this method to functionally probe GABA_AR mobility in the context of acute brain slices and find that $\alpha 1$ -containing receptors are a highly mobile population GABA_ARs that constitute a fluid portion of inhibitory synapses.

Table of Contents

Dedication	ii
Acknowledgements	iii
Chapter I: The Membrane Dynamics of GABA_A Receptors	1
Chapter II: Engineering a light-regulated GABA_A receptor	
Abstract	4
Introduction	5
Results	5
Discussion	8
Materials and methods	8
Supplemental information	9
Figures	10
Chapter III: Lateral Diffusion of GABA_ARs Studied with a Novel Technique in Acute Brain Slices	
Abstract	14
Introduction	15
Results	16
Discussion	20
Materials and methods	23
Figures	27
References	38

Dedication
To Bruce

Acknowledgements

Thank you to:

My committee chair Rich Kramer for providing a lab unafraid to try unconventional methods in pursuit of a better understanding of life.

My committee member Hillel Adesnik for insightful feedback and invaluable technical assistance.

My other committee members Dan Feldman and Frederick Theunissen for precise feedback and useful ideas.

Alex Mourot, Wan-Chen Lin, Chris Davenport, and Ming-chi Tsai, all incredible post-docs in the Kramer lab who taught me everything I know about actually doing science.

Ben Smith for calculating and designing custom optics and electronics for the microscopes.

All the members of the Kramer lab.

Mom, Dad, Maggie, Chris, and Isaiah, I'm lucky to have all of you in my life.

Chapter I: The Membrane Dynamics of GABA_A Receptors

Introduction

GABA_A receptors (GABA_ARs) are ligand-gated chloride channels that mediate most fast synaptic inhibition in the mammalian brain¹. At every level of the brain, GABA_ARs provide a counterbalancing signal to excitation, which allows precise control of neuronal membrane excitability², applies feedback to keep excitation in check in neural circuits^{3,4}, and shapes sensory signals to provide contrast⁵. Dysregulation of GABA_ARs manifests in broad range of debilitating conditions⁶ such as epilepsy³, schizophrenia⁷, and autism⁸, hinting at the ubiquity of GABA_ARs in the brain. GABA_ARs are particularly interesting in how they mediate the inhibition that shapes, sometimes in tandem with and sometimes contraposed to, the excitation that carries our neural signals forward and gives us senses and memories. Memories in particular are thought to be the result of long-lasting changes in excitation, but these changes are accompanied by massive migrations of GABA_ARs reacting to the very same signals^{9,10}. Study of inhibitory plasticity is not as mature as for the excitatory side and the full interaction of these processes is not well understood, but much is known about the underlying mechanisms of lateral mobility, surface trafficking, and synaptic clustering.

Subunits

GABA_ARs are heteropentamers consisting of two α , two β 3, and usually one γ or δ tertiary subunit^{11,12}. The most highly expressed isoforms in the brain are α 1-6, β 3, γ 1-3, and δ ¹³. The α isoform plays a dominant role in determining channel sensitivity, gating, and kinetics¹⁴. The α 1-3 subunits are broadly expressed in the brain, while the α 4 is only highly expressed in the dentate gyrus of the hippocampus and the α 6 is only found in the cerebellum¹⁵. The α 5 subunit is broadly expressed at a low level but has particularly high expression in the CA1 region of the hippocampus and the olfactory bulb¹⁶. All β subunits and γ 2 are broadly expressed, whereas the γ 1 and γ 3 are extremely rare¹⁷.

The δ subunit is only found partnered with the α 4 and α 6 and prevents incorporation into synapses¹⁶⁻¹⁹. In contrast, the α 2 and α 3 subunits are primarily found at synapses while α 1 is found distributed between the synapse, the perisynapse, and the extrasynaptic membrane¹⁶. The α 5 subunit is mostly found away from synapses²⁰, often held in extrasynaptic clusters²¹, but these clusters can disperse and the α 5 GABA_ARs can incorporate into synapses under certain conditions^{22,23}. The γ 2 and β 1-3 subunits are found at all sites within the cell, but the γ 2 in particular is necessary for synaptic clustering and gephyrin accumulation²⁴. In general, the extrasynaptic receptors are more sensitive to GABA, with α 3 being the least sensitive and α 6 the most^{14,25}.

Despite the potentially large combination of subunits constructed in the 2 α :2 β :1-tertiary configuration, relatively few are actually expressed in neurons. The α 1 β 2 γ 2 and α 2 β 3 γ 2 combinations are likely the most common across the brain^{11,26}, while the α 5 subunit is often partnered with β 3 and γ 2, especially in the hippocampus²⁷.

Membrane Trafficking and Synaptic Clustering

GABA_ARs are delivered to the neuronal membrane at extrasynaptic sites and make their way by lateral diffusion to synapses^{28,29} where they interact with a variety of proteins in a subunit-dependent manner³⁰. Gephyrin is a major protein of the inhibitory post-synapse that is necessary for a large part but not all of GABA_AR synaptic clustering^{24,31-33}. Interestingly, GABA_ARs are

recruited to expanding inhibitory synapses before gephyrin, and similarly GABA_ARs disperse from depressing synapses before gephyrin³⁴. Moreover, the accumulation of gephyrin at synapses is dependent on the $\gamma 2$ subunit²⁴, all of which indicates that gephyrin is not causal in synaptic receptor accumulation but plays a large role in stabilizing the clusters. Gephyrin directly binds to all typical synaptic subunits ($\alpha 1$ -3, $\beta 2$ -3, and $\gamma 2$) but does not interact with $\alpha 4$ -6^{33,35-37}. Gephyrin's interactions with $\alpha 2$ seem particularly important³⁸, whereas gephyrin is not required for the clustering of $\alpha 1$ GABA_ARs³⁴. Gephyrin is joined to the cytoskeleton through interactions with tubulin microtubules and actin microfilaments^{39,40}, and is itself regulated by neural activity^{41,42}.

Other key proteins involved in postsynaptic clustering include neuroligin 2 and 3, which interact with gephyrin but also provide communication with the presynaptic terminal via neurexins⁴³; dystrophin, a cytoskeletal interaction protein whose dysfunction leads to Duchenne muscular dystrophy⁴⁴; collybistin, a GDP-GTP-exchange factor that binds to gephyrin and is necessary for maintenance of synaptic clustering⁴⁵; and GABARAP, which is regulated by CaMKII and influences synaptic size and plasticity by controlling trafficking of GABA_ARs from endosomal reservoirs to the cell surface⁴⁶.

GABA_ARs are modified in an activity-dependent manner by kinases and phosphatases, a long list of which includes CaMKII, calcineurin, PKA and PKC⁹. Phosphorylation states of the GABA_ARs modulate channel kinetics⁴⁷ as well as synapse and surface stability⁴⁸, with unphosphorylated receptors (often via calcineurin^{49,50}) less likely to cluster and more susceptible to endocytosis via binding to clathrin-adaptor protein AP2^{51,52}. Conversely, receptors phosphorylated by CaMKII cluster at synapses and remain on the neuronal membrane for longer periods of time⁵³⁻⁵⁵. There are one to three phosphorylation sites on each of the β subunits and six on the $\gamma 2$ subunit (via at least 5 different kinases), but none known for the α subunits⁹. Phosphorylation of the $\beta 2$ and $\beta 3$ subunit is important for endocytosis^{51,56,57} as well as synaptic stability and gephyrin clustering⁵⁴, whereas phosphorylation of $\gamma 2$ regulates synaptic clustering²⁴.

The $\alpha 5$ -containing receptor uniquely clusters at extrasynaptic sites²⁰, held by the ERM protein radixin, which binds to actin in an activity- and rho kinase-dependent fashion²². ERM proteins are involved in a variety of actin remodeling processes, including spine expansion and shrinkage⁵⁸. Increased neural activity can cause radixin to release $\alpha 5$ GABA_ARs, allowing them to diffuse to and incorporate into synapses, resulting in increased GABA sensitivity and slower kinetics²³.

Inhibitory Plasticity

Inhibitory synapses are highly plastic^{49,59,60} and GABA_ARs and other synaptic proteins like gephyrin⁴¹ respond to many of the same signals that shape excitatory synapses⁶¹. Calcium entry into dendrites through NMDA receptors and voltage gated calcium channels regulates the activity of two important proteins, CaMKII and calcineurin. At excitatory spines, a calcium influx can activate CaMKII to produce an accumulation of AMPA receptors⁶¹. Activated CaMKII can also translocate from the spine to the dendritic shaft^{55,62} where inhibitory synapses are located and phosphorylate GABA_ARs^{9,53}, gephyrin^{41,42}, and GABARAP⁶³ to cause inhibitory potentiation⁶⁴. However, in situations with a large calcium influx that induces excitatory potentiation, the phosphatase calcineurin appears to inhibit CaMKII function as well as dephosphorylate GABA_ARs and gephyrin, resulting in inhibitory depression^{49,50}. The result is that strong stimuli tend to potentiate excitatory synapses and depress inhibitory synapses, and the opposite for weak stimuli; thus, the change in inhibition complements the excitation rather impeding it. This dynamic has potential consequences for the depolarization of nearby synapses within reach of the same

inhibitory synapse. The exact extent of this dynamic will depend on the spread and concentration of calcium within the cell and how that transduces into translocation of CaMKII.

In direct opposition to the dynamic described above, but on a slower time scale, is homeostatic regulation of GABA_ARs^{65,66}. Prolonged heightened neuronal activity leads to an overall increase of inhibition, in a mechanism that is dependent on calcium, CaMKII, and the activation of GABARAP^{63,67}, leading to insertion of new receptors into the membrane⁶⁸. Likewise, silencing of neurons leads to depletion of GABA_ARs by endocytosis, in particular those containing the $\beta 3$ subunit⁶⁹. The rapid insertion and removal of receptors from the membrane is aided by endosomal compartments that act as a reservoir of receptors⁷⁰.

Conclusions

The scene painted by our current knowledge of GABA_ARs is of a responsive and dynamic inhibitory post-synapse, gathering receptors and strength with weak rounds of activity but washing away with large waves of calcium, only to be rebuilt hours later⁷¹. In fact, this entire rearrangement can come to completion over the course of minutes^{49,60}, implying a very rapid movement of receptors in the plane of the membrane. This is borne out by a wealth of studies utilizing the single particle tracking^{72,73} method to track individual GABA_ARs labelled with quantum dots^{23,34,54,74,75}. A large range of movement speeds, expressed as diffusion rates, is consistently reported, indicating that there are fractions of relatively immobile and other highly kinetic GABA_ARs. These fractions can change with activity as a result of extrasynaptic receptors becoming trapped at synapses or internalized, and synapses shedding their receptors in mass dephosphorylation events. In addition, the mass diffusion rates of receptors can be modified by diffusion barriers forming ‘corrals’^{75–78}.

These demonstrations of GABA_AR mobility have all been performed in the context of cell culture, a devoid and flat environment compared to the rich volume of cortical neuropil that is structured by a sea of signals during development and after. The process of culturing a neuron involves stripping it of all processes into a bare soma, robbing the cell of any specialized structures it acquired during development. A much more natural experimental system is the acute brain slice, which preserves the original architecture and connectivity. Inhibitory plasticity has been observed in this environment, in both potentiation and depression of GABAergic synapse strength⁶⁰. However, to our knowledge there has never been a demonstration of GABA_AR lateral mobility in slices, let alone a report of changes accompanying activity or protein disruption. This is likely due to the difficulty of using methods like quantum dots and FRAP in the tortuous three-dimensional context of the brain. The emergence of impressive new optical methods⁷⁹ to control neurons and especially neurotransmitter receptors in slice and *in vivo*²⁵ presents an opportunity to study the phenomenon of GABA_AR lateral mobility in a new light.

Chapter II: Engineering a light-regulated GABA_A receptor

The data presented below have been published in the following article which is reprinted in full with permission:

Lin, W.-C. *et al.* Engineering a Light-Regulated GABA_A Receptor for Optical Control of Neural Inhibition. *ACS Chem. Biol.* **9**, 1414–1419 (2014).

Authors

Wan-Chen Lin, Christopher M. Davenport, Alexandre Mourot, Devaiah Vytla, Caleb M. Smith, Kathryn A. Medeiros, James J. Chambers, and Richard H. Kramer

Abstract

Optogenetics has become an emerging technique for neuroscience investigations owing to the great spatiotemporal precision and the target selectivity it provides. Here we extend the optogenetic strategy to GABA_A receptors (GABA_AR), the major mediators of inhibitory neurotransmission in the brain. We generated a light-regulated GABA_A receptor (LiGABAR) by conjugating a photo-switchable tethered ligand (PTL) onto a mutant receptor containing the cysteine-substituted α 1-subunit. The installed PTL can be advanced to or retracted from the GABA-binding pocket with 500-nm and 380-nm light, respectively, resulting in photo-switchable receptor antagonism. In hippocampal neurons, this LiGABAR enabled a robust photoregulation of inhibitory postsynaptic currents. Moreover, it allowed reversible photocontrol over neuron excitation in response to presynaptic stimulation. LiGABAR thus provides a powerful means for functional and mechanistic investigations of GABA_AR-mediated neural inhibition.

Introduction

Optogenetics, an integrated strategy that typically employs microbial opsins to overpower neuronal excitability, has become a revolutionary technique for neuroscience investigations.¹ This technique enables light to remotely manipulate neural activity with high spatial and temporal precision. Moreover, it allows photocontrol over a defined neuron type within an intact tissue or even a behaving organism⁸⁰. However, microbial opsins are functionally distinct from neuronal signaling proteins (e.g. neurotransmitter receptors for synaptic transmission), and hence they are constrained to decode neural circuits at the cellular level. To gain molecular insights into neural functions, methods that allow optogenetic control over a specific signaling mediator are highly desirable⁷⁹. Here we present a chemical-genetic approach that enables photocontrol over inhibitory neurotransmission mediated by the ionotropic type-A GABA receptors (GABA_ARs). Our approach allows light to specifically modulate a defined subtype of GABA_AR, which will help elucidate the unique functions of the receptor within a complex neural network.

The GABA_ARs, a group of neurotransmitter-gated chloride permeable channels, are therapeutic targets in psychiatric disorders⁸¹ and epilepsy⁸² owing to their inhibitory control over neuronal excitation. They are also targets for many drugs of abuse, including alcohol, barbiturates, and benzodiazepines^{12,81,83}. The GABA_ARs are heteropentameric assemblies composed of two α , two β , and one tertiary subunit (usually γ or δ , Figure 1a)^{81,83}. Among these components, the α -subunit is key in determining receptor localization and gating kinetics^{14,81,83,84}, and together with the β subunit, forms the GABA-binding site⁸¹. There are six distinct α -isoforms expressed heterogeneously in different neuron types and brain regions^{12,81,83}. Adding to this complexity, a neuron can express multiple α -isoforms which are differentially distributed in subcellular compartments⁸⁴. These findings suggest that each α -isoform has unique roles in neural signaling, and understanding their individual functions will provide key insights into GABA_AR-associated disorders and therapeutics.

Results

We have engineered a Light-regulated GABA_A Receptor (LiGABAR) by covalently conjugating a photo-switchable tether ligand (PTL) onto a receptor containing the cysteine-substituted α -subunit (Figure 1a). The PTL comprises a sulfhydryl-reactive maleimide group, a photo-switchable azobenzene core, and a ligand for the GABA-binding site (Figure 1b). It reversibly isomerizes between *cis* (twisted) and *trans* (extended) configurations upon the illumination of 380-nm and 500-nm light, respectively. Once installed near the GABA-binding pocket, the PTL can retract or advance its ligand via photoisomerization, leading to reversible photocontrol of the receptor activity. The wild-type GABA_ARs display very few extracellular cysteines which are either involved in disulfide formation or are distant from the GABA binding site. Hence, the PTL will only exert its function on an engineered receptor with an appropriately positioned cysteine, ensuring the target specificity of photoregulation within a heterogeneous population of GABA_ARs.

Our prototype PTL was designed based on previously published GABA_AR probes in which the pharmacophore muscimol is conjugated to a fluorophore or biotin via a 6-aminohexanoyl linker⁸⁵. The resulting PTL, named MAM-6, comprises a maleimide, an azobenzene, and a muscimol linked through a 6-carbon spacer (Figure 1b). Although muscimol can work as a photoaffinity probe for GABA_ARs⁸⁶, the wavelengths for MAM-6 photoisomerization are >100 nm longer than that for muscimol photolysis, incapable of triggering this side reaction. We screened MAM-6 attachment sites for the $\alpha 1$ -containing GABA_AR, the most abundant α -isoform in the brain. The screening was

carried out in *Xenopus* oocytes expressing the engineered receptors. Residues that are predicted to face the GABA-binding site were chosen for cysteine substitution (Figure 1c). Previous studies suggested that cysteine substitutions at these locations allow the mutant receptors to express normally and remain sensitive to allosteric modulators (e.g. pentobarbital and benzodiazepines)^{87,88}. These mutants are thus ideal candidates for MAM-6 conjugation.

Although muscimol is ordinarily an agonist for GABA_ARs, the mutant receptors were not activated by either 380-nm or 500-nm light after MAM-6 conjugation. Instead, MAM-6 inhibited some of the mutant receptors in a light-dependent manner, with 500 nm (*trans* MAM-6) causing a greater decrement in GABA-elicited current than 380 nm (*cis* MAM-6) did (Figure 1d and 1e and Supplementary Figure S1). This phenomenon, i.e. photo-switchable antagonism mediated by an agonist-based PTL, is similar to an observation reported previously for the nicotinic acetylcholine receptors⁸⁹, possibly caused by the PTL disrupting conformational changes required for receptor activation^{89,90}. To quantitatively evaluate each attachment site, we indexed receptor photosensitivity as the ratio of GABA-elicited current in 380 nm vs. in 500 nm (I_{380}/I_{500}). MAM-6 caused a strong photoregulation when attached at sites closer to the entrance of the GABA-binding pocket (Figure 1c and 1e). We selected $\alpha 1(T125C)$ as optimal because it allows MAM-6 to substantially inhibit the receptor in 500 nm while allowing the receptor to function normally in 380 nm (Supplementary Table S1 and Figure S1). Moreover, cysteine substitution at this location does not alter the receptor's GABA sensitivity (ref. 11 and Supplementary Table S1). These properties make $\alpha 1(T125C)$ and its resulting LiGABAR preferable for neurophysiological investigations.

We next focused on $\alpha 1(T125C)$ and investigated the structural requirements for a PTL to operate at this conjugation site. We changed the ligand and spacer moieties of MAM-6 and indexed the photoregulation effects in HEK293T cells (at 10 μM GABA; Figure 2a). The negative charge of muscimol (at physiological pH) is involved in receptor binding. Consistent with this mechanism, replacing muscimol with a neutral analogue 4-hydroxybenzylamine reduced the photoregulation effect ($I_{380}/I_{500} = 2.5 \pm 0.3$ and 1.7 ± 0.1 , $n = 6$ and 3 for MAM-6 and MAB-6, respectively; Figure 2a). Removing the 6-carbon spacer of MAM-6 suppressed photoregulation nearly completely (MAM-0; $I_{380}/I_{500} = 1.3 \pm 0.1$, $n = 4$; Figure 2a), suggesting that this spacer is important for delivering muscimol into the GABA-binding pocket. Surprisingly, substituting muscimol with 4-hydroxybenzylamine in MAM-0 boosted photoregulation, giving an effect greater than that by MAM-6 (MAB-0; $I_{380}/I_{500} = 3.4 \pm 0.4$, $n = 7$; Figure 2a).

The strong photoregulation by MAB-0 suggests a favorable interaction between its ligand moiety and the GABA-binding pocket that is specific for the *trans* configuration. The GABA-binding pocket is lined by several aromatic residues (i.e. the aromatic box)^{90,91}, and these residues may interact with 4-hydroxybenzylamide, enabling it to compete with GABA. This hypothesis was further supported by the docking of *trans* MAB-0 in a homology model. The result suggested that *trans* MAB-0 spans the distance between the attachment site and the binding pocket, delivering its terminal phenol group to the aromatic box (Figure 2b). *Trans*-to-*cis* isomerization allows the PTL to twist and withdraw the ligand, which subsequently relieves receptor antagonism. Consistent with this working model, the EC_{50} of this LiGABAR increased 8-fold when the light was switched from 380 nm to 500 nm ($10.2 \pm 2.6 \mu\text{M}$ and $84.0 \pm 19.3 \mu\text{M}$, respectively, $n = 4$ for each; Figure 2c). In addition, the EC_{50} of the conjugated receptor in 380 nm was the same as that of the wild-type ($11.4 \pm 2.2 \mu\text{M}$, $n = 4$; Figure 2c). This LiGABAR thus provides an ideal system in which the receptor can be reversibly switched between normal and inhibited states by two different

wavelengths of light. These findings also suggest that a typical agonist/antagonist is not mandatory for the PTL. When the scaffold is tethered at an appropriate position, a molecule that potentially interacts with the GABA-binding pocket could be a potent ligand, which opens a door for future PTL design. Moreover, because the GABA-binding site is highly homologous among the GABA_AR family, this strategy may be applicable to other α -isoforms to expand the toolkit.

Cis-to-trans isomerization of azobenzenes can be driven by 500-nm light or will occur spontaneously in darkness through thermal relaxation (Figure 1b and ref. 16). The rate of thermal relaxation for a *cis* azobenzene is dependent on its chemical structure and the local environment⁹². Thermal relaxation of MAB-0 (tethered to $\alpha 1$ (T125C)) was measured by a functional assay illustrated in Figure 3. GABA-elicited current was measured in HEK293T cells every 2 min in darkness after an initial response under 5 sec of 380-nm illumination. The current decreased slowly during the dark period but was fully restored by a subsequent illumination of 380-nm light, suggesting that the observed current reduction arose from thermal relaxation of *cis* MAB-0 (Figure 3a). We plotted the normalized light-sensitive current over time and fitted the data with a mono-exponential decay (Figure 3b). The half-life of *cis* MAB-0 was calculated to be 23.6 ± 2.7 min ($n = 5$) in darkness. The slow thermal relaxation of *cis* PTL makes LiGABAR bi-stable, allowing the receptor to stay in the uninhibited state for minutes after a brief pulse of 380-nm light. This feature provides a way to minimize possible adverse effects of light during the course of an experiment.

The $\alpha 1$ -GABA_AR is known to cluster at the inhibitory synapse^{84, 7}, where it detects GABA released from the presynaptic axon terminal and mediates transient postsynaptic responses^{1,93}. GABA is released into the synaptic cleft through vesicle exocytosis either spontaneously (which elicits miniature inhibitory postsynaptic current, mIPSC) or driven by action potential¹. To test whether LiGABAR enables photocontrol over synaptic inhibition, we measured the photosensitivity of mIPSCs in LiGABAR-containing neurons. Cultured hippocampal neurons were transfected with a bi-cistronic construct encoding $\alpha 1$ (T125C) and an expression marker (eGFP). The cells were subsequently treated with MAB-0 to generate LiGABARs *in situ*. As shown in Figure 4a, the amplitude of mIPSCs in a LiGABAR-containing neuron increased within 5 sec of exposure to 380-nm light and remained elevated in darkness for at least 2 min, consistent with the slow thermal relaxation of *cis* MAB-0 measured in Figure 3. The amplitude of mIPSCs decreased again upon exposure to 500-nm light. To quantify photosensitivity, we calculated the average mIPSC when MAB-0 was in either *trans* or *cis* configuration (Figure 4b). *Cis-to-trans* photoisomerization caused a $38 \pm 2\%$ decrease in the peak amplitude and a $57 \pm 4\%$ decrease in the total charge transfer ($n = 6$, Figure 4b and 4c). The robust photocontrol over mIPSCs validates the applicability of LiGABAR for neurophysiological investigations.

LiGABAR is developed for specifically probing a defined GABA_AR subtype within a complex neural system. Efficacious PTL performance should only occur when the receptor possesses the engineered subunit. Consistent with our design principle, MAB-0 treatment did not confer detectable photosensitivity onto wild-type GABA_ARs (Supplementary Figure S2). Likewise, MAB-0 treatment did not photosensitize ionotropic glutamate receptors or voltage-gated channels in neurons (Supplementary Figure S2). All together, our results suggest that light can specifically modulate the inhibitory responses mediated by the engineered GABA_AR with no apparent off-target effects.

Finally, we examined how the manipulation of LiGABAR alters neuronal excitation. Native GABA_ARs play a crucial role in preventing runaway excitation in the brain. Pharmacological

blockade of GABA_ARs^{94,95} or mutations that alter GABA_AR functions⁸² can result in epilepsy. Accordingly, we tested whether epileptiform activity can be induced by photo-antagonizing LiGABAR in an intact, *ex vivo* preparation. To express the mutant subunit, we infected a hippocampal slice with an adeno-associated virus encoding $\alpha 1$ (T125C) and an eGFP marker. After treating the slice with MAB-0, we applied a train of electrical pulses to stimulate presynaptic inputs and recorded the postsynaptic potential in 380-nm or 500-nm light. As shown in Figure 4d, the presynaptic stimulation triggered a series of postsynaptic action potentials in 380 nm. When LiGABAR was antagonized with 500-nm light, the spike train culminated in a plateau potential that is characteristic of epileptiform activity⁹⁶. Switching light back to 380 nm eliminated the effect, demonstrating the reversibility of LiGABAR modulation. This result suggests that optical perturbation of LiGABAR function is sufficient to cause a profound impact on neuronal excitation.

Discussion

In summary, our approach enables light to manipulate the inhibitory events mediated by a designated subtype of GABA_AR. LiGABAR inherits two renowned benefits from opsin-based optogenetics, namely the fine spatiotemporal precision of optical manipulation and the capability of targeted gene expression using cell-type specific promoters^{79,80}. PTL photoisomerization can alter neuronal activity within milliseconds reversibly and reliably⁹⁷, suitable for accurate neurophysiological manipulations. Aside from these advantages, LiGABAR differs from microbial opsins in that it allows direct photocontrol over a genuine mediator in neuronal signaling. GABA_ARs mediate inhibitory neurotransmission in the nervous system, with different subtypes exerting distinct biophysical properties and cellular/subcellular distributions^{14,81,83,84}. The biochemical specificity of photocontrol makes LiGABAR favorable for probing the function/distribution of a GABA_AR subtype within a neuron or a neural circuit. Compared to diffusible caged agonists or photochromic modulators (i.e. optopharmacology)⁷⁹, the use of LiGABAR is more technically demanding due to the requirement of two exogenous components (mutant subunit and PTL). However, LiGABAR enables advanced investigations that aim to explore a specific receptor and/or neuron subtype in a complex system, which cannot be achieved with existing optopharmacology agents because of their lack of target specificity. LiGABAR thus presents a unique opportunity for understanding the mechanism of neural inhibition, and ultimately provides new insights into brain function and dysfunction.

Methods and Materials

Buffer formulations are available in Supporting Information. Animal care and experimental protocols were approved by the University of California Berkeley Animal Care and Use Committee.

Receptor expression and PTL treatment

***Xenopus* oocytes.** RNA was prepared with the mMessage mMachine T7 kit (Ambion). Defolliculated *Xenopus* oocytes were injected with 2.5-20 ng of mRNA in 50 nL H₂O in a ratio of 1:1 ($\alpha 1$: $\beta 2$). The injected oocytes were incubated at 18 °C (in OR1 buffer) and subjected to two-electrode voltage-clamp recording 1-3 days after RNA injection. To screen MAM-6 attachment sites, oocytes expressing each mutant receptor were incubated with 50 μ M MAM-6 for 0.5–1.5 h prior to recording.

HEK293T cells. Cells were maintained in Dulbecco's Minimum Essential Medium (Gibco) supplemented with 10% fetal bovine serum (Gibco) at 37 °C and 5% CO₂. Cells were plated at $18-24 \times 10^3$ cells/cm² on poly-L-lysine coated coverslips and transfected by calcium phosphate precipitation. A total of 1.1 µg DNA per coverslip ($\alpha:\beta:\gamma:eGFP = 0.15:0.15:0.75:0.05$) was used. Recordings were carried out 36–48 hours after transfection. Prior to recording, cells (in external recording solution) were treated with dithiothreitol (DTT; 3 mM, 5 min), incubated in fresh external recording solution (5 min), and then treated with PTL (25 µM, 20 min) at room temperature in the dark.

Cultured hippocampal neurons. Primary cultures of neonatal rat hippocampal neurons were prepared and maintained following previously described procedures.⁹⁸ Neurons were transfected via calcium phosphate precipitation (1.2 µg of the bi-cistronic pAAV construct per well) 6-8 days after preparation. Recordings were carried out 1-2 weeks after transfection. Prior to recording, neurons (in external recording solution) were treated with tris(2-carboxyethyl)phosphine (TCEP; 5 mM, 5 min), incubated in fresh external recording solution (5 min), and then treated with MAB-0 (25 µM, 20 min) at room temperature in the dark.

Organotypic slice cultures. Sprague-Dawley rat pups (postnatal day 8) were anaesthetized and decapitated. Hippocampi were removed and sliced into 350 µm-thick sections. Slices were maintained at 34 °C on cell culture inserts in Neurobasal-A medium (Invitrogen) supplemented with 20% horse serum (Thermo Scientific), 0.03 units/ml insulin (Sigma), 0.5 mM ascorbic acid (Sigma), 1X Gluta-Max (Invitrogen), 80 units/ml penicillin (Sigma), 80 µg/ml streptomycin (Sigma), and 25 mM HEPES. One day after preparation, slices were injected with AAV9 (7.5×10^{12} vg mL⁻¹) encoding the bi-cistronic construct of GFP-2A- $\alpha 1$ (T125C). The CA1 pyramidal cell body layer was injected at 3–7 sites/slice with 100 nL of virus. Recordings were carried out 5–14 days post-injection. Prior to recording, slices were incubated for 2 min with 1 mM TCEP in artificial cerebrospinal fluid (ACSF), washed, and incubated with 25 µM MAB-0 in ACSF for 30 min at room temperature.

Supporting Information

Details of PTL synthesis, preparation of plasmids and virus, electrophysiology, and molecular modeling. This material is available free of charge via the Internet at <http://pubs.acs.org>.

Acknowledgement

We thank Prof. Cynthia Czajkowski (University of Wisconsin) for sharing GABA_AR cDNAs and Dr. Kathleen Durkin (University of California, Berkeley) for helpful assistance in molecular modeling.

The authors declare no competing financial interests.

Figures

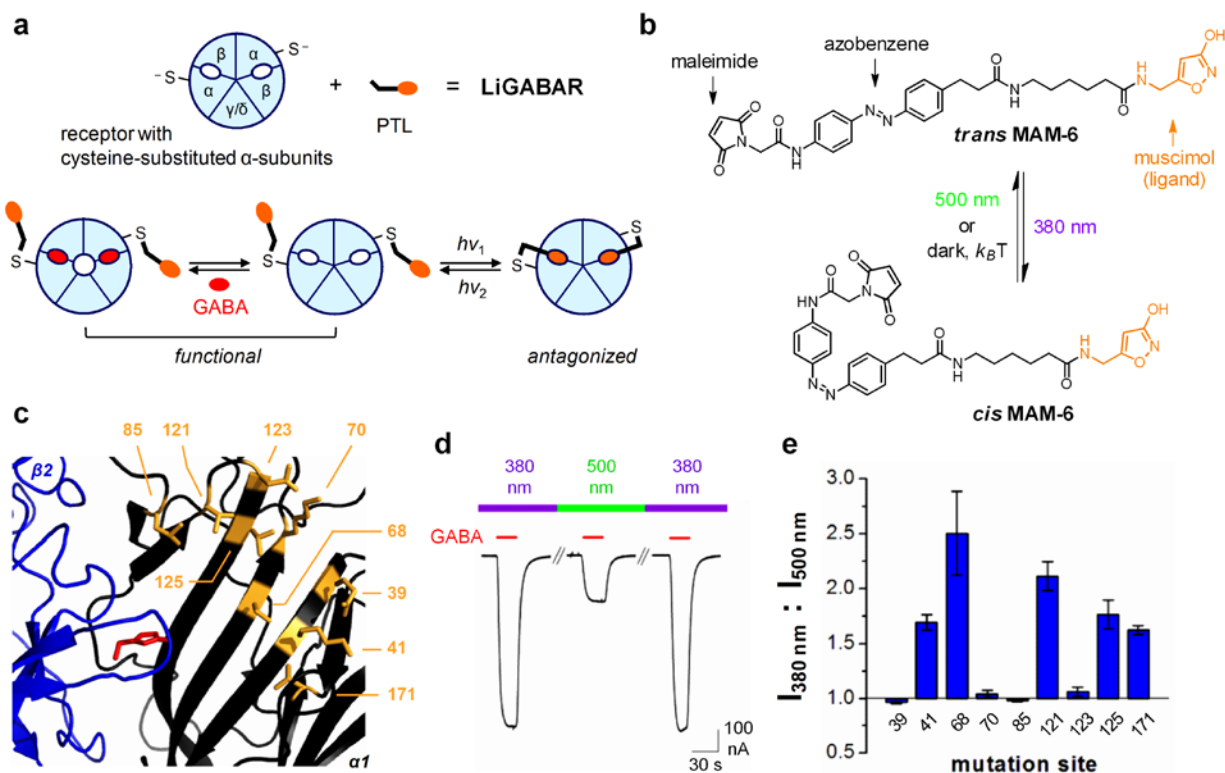


Figure 1. Engineering of the light-regulated GABA_A receptor (LiGABAR). (a) A LiGABAR is generated by conjugating a photo-switchable tethered ligand (PTL) onto a receptor comprising the cysteine-substituted α -subunits (top). In the case of photo-switchable antagonism (bottom), the installed PTL reversibly isomerizes between two states in response to two different wavelengths of light, with one enabling and the other preventing GABA binding (and the subsequent gating of the transmembrane channel). (b) The structure and photochemistry of MAM-6 (the prototype PTL). (c-e) Identification of MAM-6 attachment sites in the $\alpha 1$ subunit. (c) Distribution of the tested cysteine-substituted residues (orange; sidechain in sticks) in a homology model of $\alpha 1\beta 2$.²⁴ The GABA-binding site is indicated by a docked muscimol (red). (d) Representative traces showing reversible photoregulation of GABA-elicited currents by the tethered MAM-6. Mutant = $\alpha 1$ (S68C). (e) Photoregulation of mutant receptors after MAM-6 conjugation. Each mutant was co-expressed with the wild-type $\beta 2$ in *Xenopus* oocytes. The photoregulation index (mean \pm SEM) was measured at 3 μ M GABA, -80 mV. A ratio of 1 indicates no photosensitivity of the tested receptor.

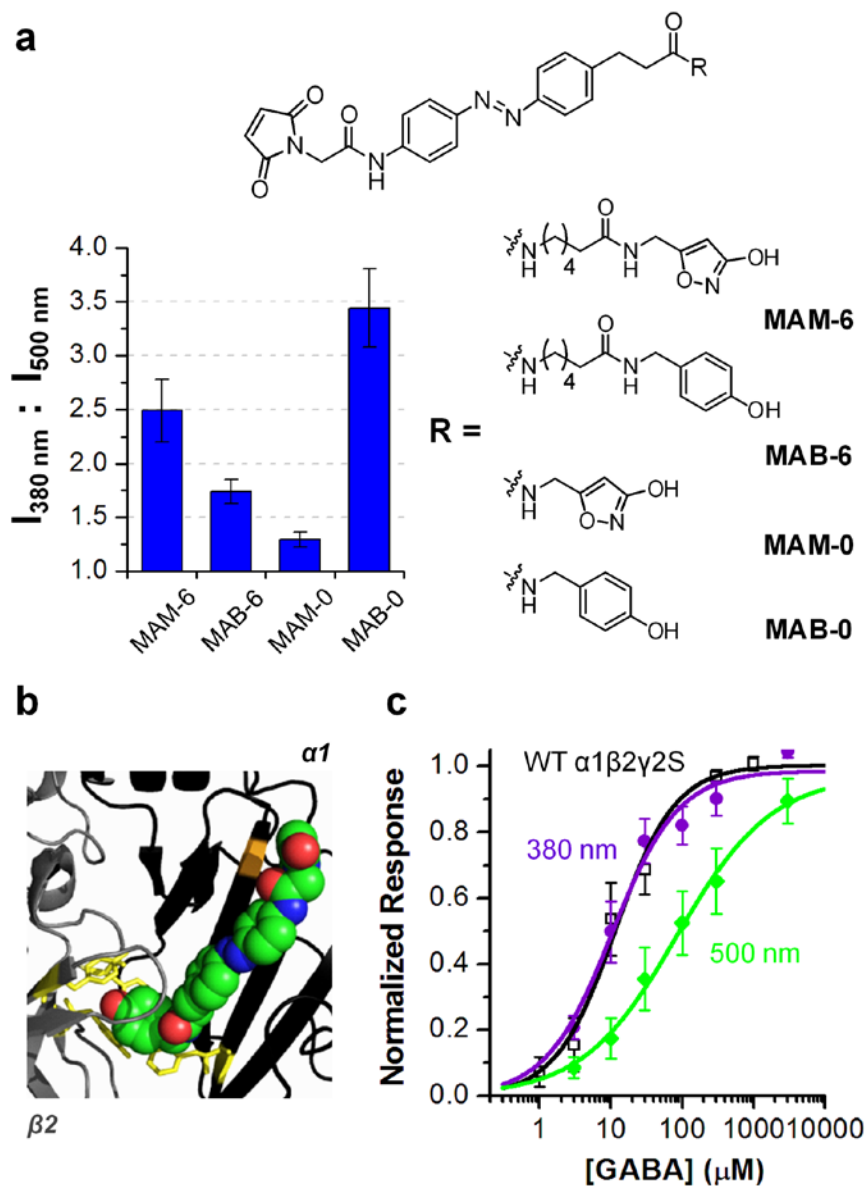


Figure 2. Characterizations for the $\alpha 1(\text{T}125\text{C})$ -based LiGABAR. (a) Structure-activity investigation of the PTL modules. Photosensitivity of each conjugated $\alpha 1(\text{T}125\text{C})\beta 2\gamma 2\text{S}$ was indexed at $10 \mu\text{M}$ GABA. $n = 3 \square 7$. (b) A representative docking pose of *trans* MAB-0 (spheres) in a homology model of $\alpha 1(\text{T}125\text{C})\beta 2$ complex. A positional constraint was applied to mimic the tethering of *trans* MAB-0 at $\alpha 1(\text{T}125\text{C})$ (orange). Residues of the aromatic box ($\alpha 1\text{F}64$, $\beta 2\text{Y}97$, $\beta 2\text{Y}157$, and $\beta 2\text{Y}205$) are shown as yellow sticks. (c) Dose-response curves for the wild-type $\alpha 1\beta 2\gamma 2\text{S}$ (black) and MAB-0 conjugated $\alpha 1(\text{T}125\text{C})\beta 2\gamma 2\text{S}$ under 380-nm (purple) and 500-nm (green) illumination. Data are presented as mean \pm SEM. $n = 4$ for all three curves. Recordings were carried out in HEK293T cells held at -70 mV .

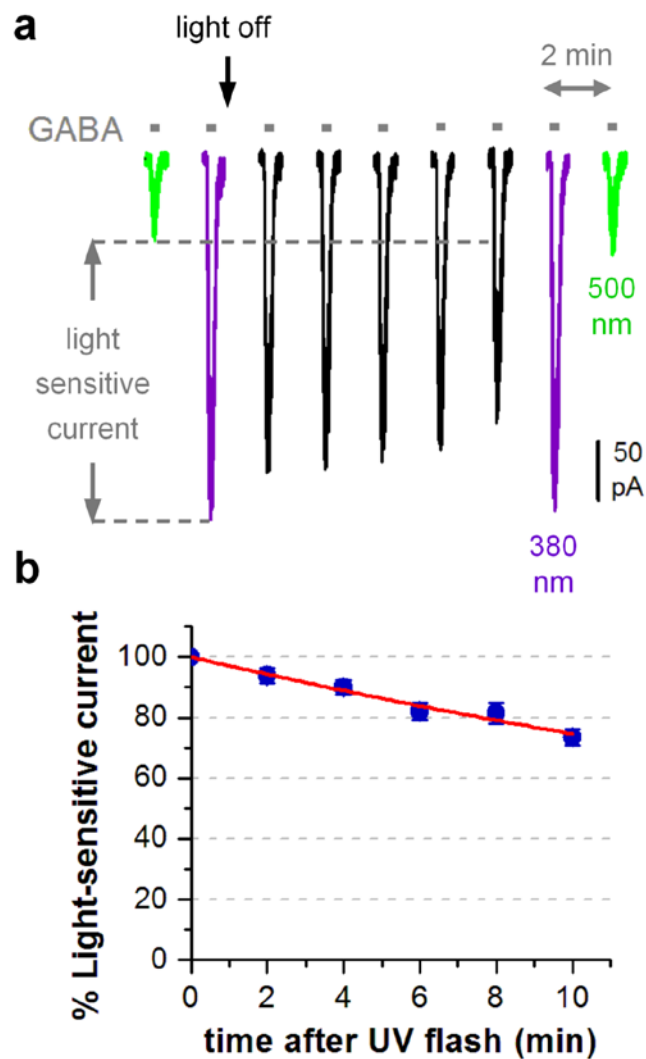


Figure 3. Thermal relaxation of the tethered MAB-0. (a) A representative cell (with MAB-0 conjugated $\alpha 1(T125C)\beta 2\gamma 2S$) showing the slow current reduction in darkness after an initial response measured in 380 nm. [GABA] = 10 μ M. (b) Group data (mean \pm SEM, n = 5) showing the time course of thermal relaxation, plotted as changes in the normalized light-sensitive current component (defined in 3a) and fitted with a single-exponential decay (red curve). Recordings were carried out in HEK293T cells held at -70 mV.

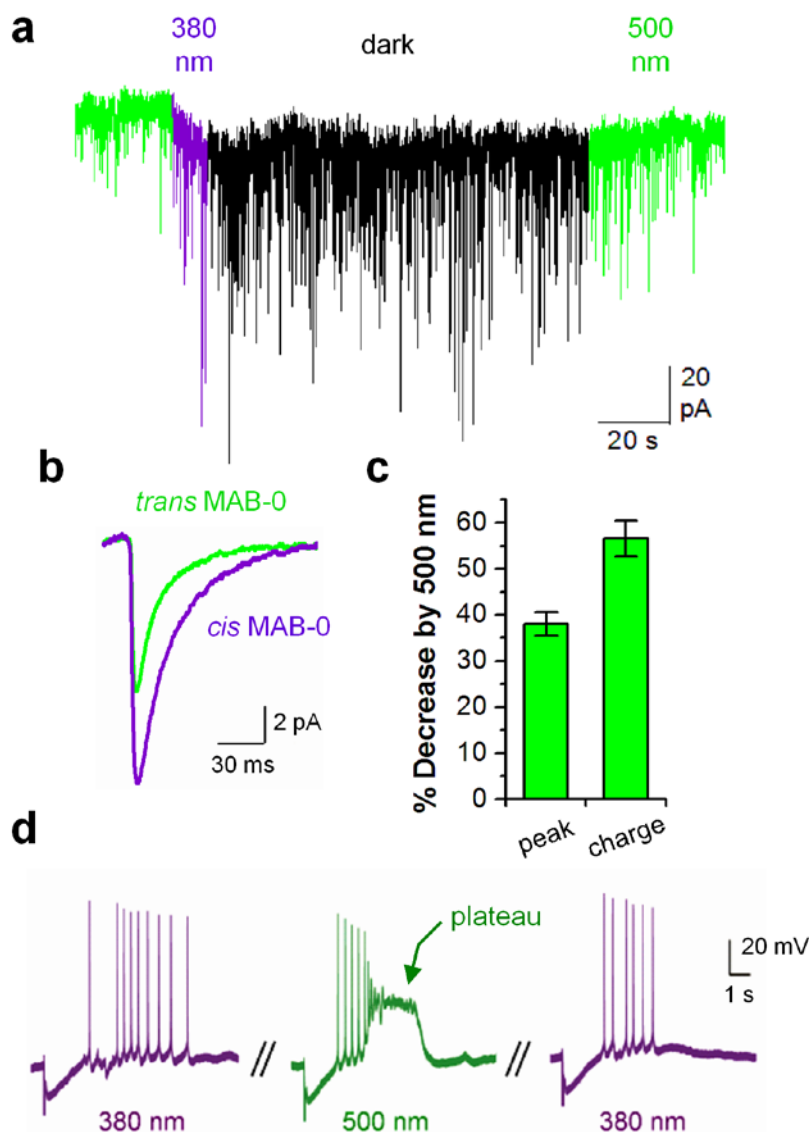


Figure 4. $\alpha 1$ -LiGABAR enables photocontrol over miniature inhibitory postsynaptic currents (mIPSCs) and epileptiform formation in hippocampal neurons. (a) A representative continuous trace from a cultured hippocampal neuron containing $\alpha 1$ -LiGABAR. Cell was held at -60 mV and was treated with inhibitors of voltage-gated sodium channels and ionotropic glutamate receptors. (b) Average mIPSC traces from the same cell shown in (a). The green and purple traces represent average mIPSCs when MAB-0 was in the *trans* (500 nm) and *cis* (380 nm + dark) configuration, respectively. (c) Quantification of mIPSC photoregulation (mean \pm SEM) as the percent decrease when MAB-0 was switched from *cis* to *trans*. The total charge transfer was measured by integrating the area of average mIPSC.¹⁷ (d) Photocontrol over neuron excitation in a hippocampal slice. Current-clamp recording was carried out in a LiGABAR-containing CA1 pyramidal neuron. Illumination of 500-nm light resulted in an “epileptic” plateau potential that was subsequently eliminated by 380-nm light.

Chapter III: Lateral Diffusion of GABA_ARs Studied with a Novel Technique in Acute Brain Slices

Author contribution

Experiments conceived Caleb Smith and Rich Kramer, performed and analyzed by Caleb Smith

Abstract

Previous studies of GABA_A receptors (GABA_ARs) in neuronal cultures have shown that the receptors are mobile on the cell surface and are incorporated into inhibitory synapses via lateral diffusion in the plane of the membrane. Moreover, GABA_ARs are plastic, responding to changes in neuronal activity by altering their apparent lateral diffusion rates and by insertion or removal of GABA_ARs from the membrane, resulting in long term potentiation or depression of inhibitory neurotransmission. However, almost all previous work on GABA_AR mobility has been done in the context of neuronal cultures, where dendrite morphology and molecular composition have been radically altered from *in vivo* conditions, and where the primary method has been single particle tracking of individual GABA_ARs modified with quantum dots. In this study we make use of LiGABAR technology to pioneer a novel electrophysiological technique for measuring GABA_AR mobility, which we call CREAP. We use this method to functionally probe GABA_AR mobility in the context of acute brain slices. We find that α 1-containing receptors are a highly mobile population GABA_ARs that constitute a fluid portion of inhibitory synapses.

Introduction

GABA_A receptors (GABA_ARs) are chloride-conducting ligand-gated ion channels that mediate most fast inhibitory transmission in the mammalian nervous system¹ and are essential for normal neural function at the circuit^{3,8}, whole-brain³, and behavioral levels⁷. GABA_ARs are heteropentamers that assemble from two α , two β , and one tertiary (γ or δ) subunit in the brain^{11,26}. The α subunits are major determinants of receptor affinity for GABA¹⁴, channel kinetics, and subcellular positioning^{16,17}. Six different α subunits are known, with α 1-3 often considered the synaptic receptors responsible for ‘phasic’ inhibition, and α 4-6 considered extrasynaptic receptors generating ‘tonic’ inhibition¹.

This view is elaborated by the recognition that GABA_ARs are highly dynamic and move fluidly between synaptic and extrasynaptic zones via lateral diffusion. It is in fact this dynamic that allows inhibitory synapses to rapidly potentiate and depress by accumulating or shedding receptors and by limiting the available pool of synaptic receptors via trafficking to and from the membrane^{9,10,30,99,100}. These changes in GABAergic strength are mediated by many of the same signals that shape excitatory synapses: calcium entry through NMDA receptors and voltage-gated calcium channels and subsequent phosphorylation of proteins by CaMKII^{53,67} or the reverse by calcineurin^{49,50}. In general, increased phosphorylation states of GABA_ARs, as well as their associated synaptic scaffolds like gephyrin, are associated with synaptic stability, decreased diffusion rates of receptors as they are trapped in synaptic zones, and exocytosis of new receptors^{10,30}.

GABA_AR lateral mobility has been extensively studied with single-particle tracking of quantum dots^{72,77}, which show a large range of diffusion rates over five orders of magnitude – from freely diffusing on the membrane to solidly immobilized in the synapse, and many at intermediate rates, slowed and corralled by synaptic proteins^{23,34,54,74,75,101}. These experiments have exposed interesting consequences of lateral diffusion, such as desensitized receptors spreading to other nearby synapses¹⁰². However, these experiments were all performed in the conditions of neuronal cell culture, making it hard to predict how the effects will play out in the intact brain. The same is true for the other major method used to study protein mobility, fluorescence recovery after photobleaching (FRAP), in which a spot of fluorescently-labelled protein is bleached with a laser and then monitored for return of fluorescence due to lateral diffusion^{32,75,103}.

To investigate these questions in a more natural situation such as acute brain slice or even *in vivo*, we developed the LiGABAR set of tools to modulate GABA_ARs with spatial and temporal precision^{25,79,104}. The LiGABAR consists of a GABA_AR α isoform with a strategically placed cysteine point mutation, allowing the covalent conjugation of a photoswitchable tethered ligand (PTL). Before PTL attachment, the receptor behaves like a wildtype GABA_AR. However, once the LiGABAR has been formed, we can competitively antagonize the receptor with longer wavelengths of visible light and completely relieve antagonism with shorter wavelengths. We created a transgenic knock-in α 1 photoswitch-ready mouse (α 1 PhoRM) to express the mutant receptor at endogenous levels and distributions²⁵. We also synthesized a new ‘thermostable’ PTL to grant us bi-stable photo-inhibition that persists over a longer period of time (unpublished).

By applying small pulses of GABA to the apical dendrite of hippocampal CA1 pyramidal cells and blocking only the receptors activated by the GABA with a flashed spot of light (much like bleaching a spot in FRAP), we were able to record the lateral diffusion of unblocked receptors into the GABA pulse as a rise in current. Using this novel technique which we call current recovery

after photo-inhibition (CREAP), we show that $\alpha 1$ GABA_ARs constitute a relatively fluid portion of synaptic receptors.

Results

LiGABARs can be photo-inhibited with spatial precision

We made acute brain slices from $\alpha 1$ PhoRM mice and applied the thermostable PTL PAG-1C-G1 (unpublished) to generate the functional $\alpha 1$ LiGABARs. We used an upright slice microscope equipped with custom optics and a digital micromirror device which allowed us to project arbitrary patterns of LED-generated light onto our slices (Figure 1A). We utilized iontophoresis to apply small pulses of GABA to the apical dendrites of CA1 hippocampal pyramidal cells at a distance approximately 100 μm from the soma, eliciting chloride currents which we recorded from a patch pipette at the soma (Figure 1A and B). We projected full-field light of 385 nm or 460 nm to unblock or block all the LiGABARs in the slice, respectively, and determine the maximal degree of photo-inhibition for each cell.

To measure the spatial extent of the GABA application, we projected 460 nm spots of decreasing diameter centered on the dendrite at the position of the iontophoresis pipette tip. The photo-inhibition significantly decreased with spot diameters of less than 20 μm ($p < 0.001$, t-test, $n = 7$), indicating that this was the size of the iontophoretic GABA pulse (Figure 1D). Therefore a 20 μm spot of light allowed us maximally modulate the LiGABARs activated by the iontophoresis without affecting the LiGABARs outside of the pulse. We checked the spatial precision of our light spot by moving a 30 μm spot orthogonal to the dendrite (Figure 1E). We found a sharp drop-off of photo-inhibition that closely matched the expected geometry, indicating that our projected light was precise and focused ($p < 0.001$, t-test, $n = 5$).

CREAP: A novel technique for measuring membrane diffusion of neurotransmitter receptors

Taking inspiration from FRAP, we developed an analogous technique which we dubbed current recovery after photo-inhibition, or CREAP. The experiment was performed as follows (Figure 1A and B). First, we measured maximal photo-inhibition of iontophoresis-evoked currents with full-field light at 460 and 385 nm. Next, we confirmed that a 20 μm spot of 460 nm light allowed maximal photo-inhibition; if not, we adjusted the strength of the iontophoresis pulse to be as spatially large as possible while still reaching maximal photo-inhibition, ensuring a spatial match between GABA application and spot size. To initiate the recovery measurement, we projected full-field 385 nm light to unblock all LiGABARs followed immediately by the 460 nm spot to block the LiGABARs only at the iontophoresis site. We then left the slice in the dark and continued to pulse GABA at regular intervals for 15 minutes (Figure 1B right, 1C). Finally, at the end of 15 minutes we projected full-field light to again measure the maximal extent of photo-inhibition. By comparing the average current at the end of the dark period to the average maximally unblocked and blocked currents, we were able to measure the degree of recovery of the current due to the lateral diffusion of unblocked LiGABARs into the 20 μm spot region.

$\alpha 1$ GABA_ARs are mobile in the membrane

We performed CREAP with the $\alpha 1$ PhoRM mouse and found a significant $29.5 \pm 11.5\%$ increase of the current at the end of the 15-minute recovery period ($p = 0.036$, t-test, $n = 8$) (Figure 2A). Fitting this recovery with an exponential function, we estimated a recovery time constant of $\tau = 142$ s.

NMDA treatment decreases $\alpha 1$ GABA_AR mobility

A large body of research has shown that GABA_ARs are plastic, and inhibitory synapses undergo activity- and calcium- dependent changes in strength^{9,10,30,99,100}. To study the effect of activity changes on $\alpha 1$ LiGABAR mobility, we applied 50 μ M NMDA with 5 μ M glycine to our slice for 2-3 minutes and afterward performed CREAP. Compared to control slices, this treatment caused a significant rise in the AMPA/NMDA ratio ($p = 0.009$, two-tailed t-test) (Figure S1), consistent with excitatory LTP and inhibitory LTD. We were not able to detect any recovery of current after NMDA treatment ($p = 0.423$, t-test, $n = 3$), indicating that the treatment likely caused a small decrease of mobility (Figure 2B). The maximal photo-inhibition increased to $19.3 \pm 2.12\%$ from $12.72 \pm 2.54\%$ as a result of treatment ($p = 0.19$, U-test) but it did not change during the experiment ($p = 1$, U-test).

Disruption of the actin cytoskeleton decreases $\alpha 1$ GABA_AR mobility

Actin is a major component of the cytoskeleton that interacts with elements of the inhibitory post-synapse, including gephyrin⁴⁰. Disruption of actin polymerization with the drug cytochalasin D has been shown in culture to reduce the size of GABA_AR clusters and disperse GABA_ARs across the membrane^{39,48,105-107}. We applied 10 μ M cytochalasin D to our slices for 2 hours before performing CREAP. In this condition, we were not able to detect any recovery of current ($p = 0.105$, t-test, $n = 8$) (Figure 2B).

Ablation of gephyrin does not increase $\alpha 1$ GABA_AR mobility

Gephyrin is a major anchoring protein found at inhibitory synapses that binds to all major synaptic subunits^{33,35-37}. It is necessary to form stable inhibitory synapses and its disruption leads to decreased IPSCs and increased diffusion of synaptic GABA_ARs^{24,31-33}, although it is not necessary for all forms of synaptic clustering³⁴. We removed gephyrin from neurons by injecting the $\alpha 1$ PhoRM mouse with an adeno-associated virus encoding a gephyrin-targeting intrabody tethered to an E3 ligase (AAV-GFE3), causing gephyrin to become ubiquitinated and ablated from infected cells¹⁰⁸.

In cells infected with GFE3, we measured a significant recovery of current ($p = 0.017$, t-test, $n = 6$), but this recovery was not different from uninfected cells ($p = 0.099$, one-way ANOVA) (Figure 2B). This result indicates that gephyrin likely did not play a significant role in tethering the $\alpha 1$ LiGABARs in the $\alpha 1$ PhoRM mouse.

Viral overexpression of $\alpha 1$ LiGABAR reduces mobility

In our experience, viral overexpression of GABA_AR α subunits over a wildtype background causes greater incorporation of that subunit into the synaptic population without an increase of total inhibition²⁵. In the $\alpha 1$ PhoRM mouse, we saw $29.41 \pm 1.37\%$ photo-inhibition of electrically-evoked IPSCs ($n = 8$), while with overexpression we see $46.48\% \pm 2.51\%$ ($n = 5$) (Figures 2C and 3C). Likewise, with iontophoresis-evoked currents we measure $12.72 \pm 2.54\%$ photo-inhibition in the $\alpha 1$ PhoRM mouse ($n = 8$), and $32.81 \pm 4.22\%$ with $\alpha 1$ overexpression ($n = 9$).

We performed CREAP on cells infected with AAV- $\alpha 1$ -LiGABAR and found a non-significant recovery of $3.81 \pm 1.78\%$ ($p = 0.065$, t-test, $n = 9$) (Figure 3A), which was significantly different from the $\alpha 1$ PhoRM result ($p = 0.009$, one-way ANOVA) (Figure S2). This recovery with overexpression constituted $2.28 \pm 1.02\%$ of the total iontophoresis current, while in the $\alpha 1$ PhoRM

the recovery was $6.14 \pm 1.75\%$ of the total ($p = 0.124$, U-test) despite the much lower level of photoinhibition (Figure S2B). We therefore saw reduced recovery both as a fraction of $\alpha 1$ -LiGABAR-mediated current and overall as a result of overexpression.

We repeated the NMDA treatment with $\alpha 1$ LiGABAR overexpression and found no significant recovery of current ($p = 0.177$, t-test, $n = 6$), a result that was indistinguishable from control ($p = 0.454$, one-way ANOVA) (Figure 3B). However, we did see a decrease in photo-inhibition of iontophoresis as a result of treatment ($32.8 \pm 4.22\%$ in control compared to $23.58 \pm 3.72\%$ with NMDA, $p = 0.012$, U-test), the opposite direction compared to the $\alpha 1$ PhoRM.

We applied cytochalasin D to AAV- $\alpha 1$ -liGABA_AR-expressing slices and found a small but significant recovery of $7.97 \pm 2.53\%$ ($p = 0.009$, t-test, $n = 12$) (Figure 3B). We also tested the effect of the microtubule-disrupting drug nocodazole, which has been shown to reduce GABA_AR clustering and disperse receptors across the membrane^{39,109,110}. We applied $10 \mu\text{M}$ nocodazole to the slices for 2h and saw a significant current recovery of $10.36 \pm 4.14\%$ ($p = 0.031$, t-test, $n = 7$) (Figure 3B). Neither cytoskeleton drug treatment was significantly different to control ($p = 0.362$, one-way ANOVA), indicating a small effect.

Viral overexpression of $\alpha 5$ LiGABAR causes synaptic incorporation and immobilization

The $\alpha 5$ GABA_AR subunit is particularly interesting because it is expressed at relatively high levels in the CA1 region of the hippocampus¹⁶, yet its contribution to synaptic currents is controversial and appears small at best^{20,21,111,112}; tonic chloride current in CA1 pyramidal cells has been largely attributed to $\alpha 5$ -containing receptors^{113,114}. Single particle tracking experiments with quantum dots show that $\alpha 5$ -containing GABA_ARs are more mobile than those with $\alpha 1$ or $\alpha 2$ ²³. In the $\alpha 5$ LiGABAR PhoRM mouse (unpublished), we observed photo-inhibition of tonic currents in voltage clamp and photo-modulation of membrane potential in current clamp, resulting in control of the spontaneous spiking rate (Figure S3A). However, in normal conditions we saw only a small contribution of $\alpha 5$ LiGABAR to synaptic currents at distal dendrites and no contribution to perisomatic synapses (Figure S3D and S3B). We also saw no photo-inhibition of iontophoresis-evoked currents (Figure S3C). Viral overexpression of $\alpha 5$ LiGABAR led to strong synaptic incorporation, with $45.83 \pm 2.44\%$ photo-inhibition of perisomatic electrically-evoked IPSCs ($n = 8$) (Figure 4C) and $33.46 \pm 2.96\%$ ($n = 9$) photo-inhibition of iontophoresis-evoked currents.

We performed CREAP on cells infected with AAV- $\alpha 5$ -LiGABA_AR and found a non-significant recovery of $1.85 \pm 1.41\%$ ($p = 0.225$, t-test, $n = 9$) (Figure 4A). This result was significantly different from recovery in the $\alpha 1$ PhoRM but not from $\alpha 1$ LiGABAR overexpression ($p = 0.009$, one-way ANOVA) (Figure S2). We treated the slices with NMDA as previously described and saw no recovery ($p = 0.5$, t-test, $n = 2$) (Figure 4B). We again applied the cytoskeleton-disrupting drugs cytochalasin D and nocodazole to slices for 2 hours before performing CREAP. Cytochalasin D did not result in a recovery ($p = 0.194$, t-test, $n = 5$), but with nocodazole we did see a large recovery of $24.1 \pm 4.4\%$ ($p = 0.001$, t-test, $n = 7$) which was significantly different to control ($p = 0.0004$, one-way ANOVA) (Figure 4B).

Radixin is an actin-binding protein of the ERM family that binds to $\alpha 5$ GABA_ARs in its active form and is hypothesized to hold $\alpha 5$ in extrasynaptic clusters as a reservoir^{22,23}. Upon dephosphorylation, radixin releases $\alpha 5$ GABA_ARs into the extrasynaptic space where they diffuse at a higher rate and incorporate into synapses²³. In culture conditions, overexpressing a dominant-negative radixin mutant (T564A) is reported to cause the disappearance of extrasynaptic $\alpha 5$ -

containing clusters, increase of $\alpha 5$ diffusion rates, and incorporate of $\alpha 5$ GABA_ARs into synapses²³. We co-injected AAV- $\alpha 5$ -LiGABA_AR along with a virus encoding a dominant-negative radixin (AAV-Rdx) and performed CREAP on double-infected cells. We saw a significant $12.2 \pm 4.6\%$ recovery of current ($p = 0.047$, t-test, $n = 6$) (Figure 4B).

Modeling lateral mobility of GABA_ARs using Fick's laws of diffusion

GABA_ARs are mobile in the plane of the membrane and therefore their movement can be described with diffusion constants⁷³, which have been extensively reported using single particle tracking of receptors labeled with quantum dots^{23,34,54,74,75,101}. Diffusion of particles can be predicted by Fick's laws of diffusion, which describe the change of particle density as a function of time, space, and diffusion constant. We utilized a standard formulation of this model to simulate CREAP along a dendrite (Figure 5A) using diffusion rates gleaned from the quantum dot studies. We validated the model by using reported diffusion rates and experimental parameters to reproduce published FRAP data⁵⁴ (Figure S4).

We calculated the expected recovery over time for $\alpha 1$ and $\alpha 5$ GABA_ARs (Figure 5B, Table S1). The model predicted a recovery of 28.3% for $\alpha 1$ LiGABAR, similar to our experimental result of 29.5% with the $\alpha 1$ PhoRM (Figure 5C). We found a slightly faster recovery time constant with our fitted experimental data ($\tau = 149$ s) compared to the model ($\tau = 196$ s). By scaling the reported diffusion rates and distributions to better match the experimental data, we estimate the average diffusion rate of the LiGABARs in the $\alpha 1$ PhoRM mouse at $\sim 0.075 \mu\text{m}^2/\text{s}$ ($\tau = 168$ s).

While the QD data matched well with our $\alpha 1$ PhoRM results, it did not describe the situation with viral overexpression of the $\alpha 1$ and $\alpha 5$ LiGABARs, where we only saw recoveries of $3.81 \pm 1.78\%$ and $1.85 \pm 1.41\%$, respectively. A common report in single particle tracking studies of GABA_ARs is an 'immobile' fraction of particles¹¹⁵. The lowest rates generally reported in single particle tracking experiments for GABA_ARs are $0.0001 \mu\text{m}^2/\text{s}$, meaning that the 'immobile' fraction diffuses at a rate slower than this. In the model, using this single rate resulted in a 1.33% recovery over a 15-minute period. We incorporated an immobile fraction of synaptic receptors into our model and found a decreasing recovery as a result (Figure 5D). With the diffusion rate of all synaptic receptors set to zero, the remaining recovery was a function of extrasynaptic GABA_AR density and diffusion rate. A very low extrasynaptic LiGABAR density was necessary to achieve the experimental recoveries with overexpression, indicating that extrasynaptic receptors likely constituted a very small fraction of the overexpressed LiGABARs (Figure 5E) but a much larger fraction of the receptors in the $\alpha 1$ PhoRM.

We attempted to estimate the diffusion rate of the viral overexpression conditions by calculating recovery as a function of a single average diffusion rate (Figure 5F). We found that an average synaptic diffusion rate of $\sim 0.0005 \mu\text{m}^2/\text{s}$ or lower was necessary to limit recovery to the experimental levels if we assumed that the extrasynaptic density of LiGABARs was negligible.

We posed a theoretical question: what magnitudes of diffusion rates might we expect for synaptic receptors? We again used Fick's laws of diffusion, this time to create a model of a given length of dendrite with synaptic and extrasynaptic densities and areas estimated from reported values^{54,59,116-118} (Figure S5A, Table S2). Using synaptic diffusion rate as a variable, we calculated the equilibrium distribution of receptors between the synaptic area and the extrasynaptic membrane (Figure S5B). As expected, we found that increasing synaptic diffusion rates resulted in the synapse shedding receptors into the extrasynaptic membrane. We estimated the diffusion rate at

which the synapse was half-occupied by receptors in a typical dendrite (D_{SYN50}) at $\sim 0.0005 \mu\text{m}^2/\text{s}$. We then calculated D_{SYN50} as a function of the number of receptors per synapse, dendrite diameter, and the extrasynaptic receptor diffusion rate (Figure S5C-E).

Discussion

In this paper we introduced a novel method, CREAP, for measuring the lateral mobility of GABA_ARs in acute brain slices. It is worth discussing the limits and applications of the technique, and how it compares to other currently available methods. We will also discuss the cytoskeletal tethering of GABA_ARs, diffusion modeling of membrane receptors, and the implications from experiments and models to the roles of different GABA_AR subunits.

A primary motivation for developing CREAP was the lack of available techniques for monitoring lateral mobility of receptors in more intact experimental systems such as brain slices and *in vivo*. There is a great wealth of scientific literature about GABA_AR mobility, but the work has been done almost entirely in the context of neuronal cultures. When neurons are cultured, the brain tissue is triturated and the neurons are completely stripped of all processes, leaving bare somata to be plated on a flat surface. Over the following several weeks of culture conditions, the neurons spontaneously regrow their axons and dendrites and form functional synapses with other cultured neurons. Culture provides a way to study the interactions of proteins and genes in a controlled and practical environment and has been essential to the progress of the biological sciences. But neuronal culture does not recapture the exquisite dance of development and it does not recapitulate the byzantine mosaic of cortical neuropil. Put another way, culture can tell us the rules but it doesn't explain how events actually play out in our brains.

CREAP experimental parameters

If the primary attraction of CREAP is that it can be done in an acute brain slice, its main drawbacks are technical. The first experimental choice is the method of locally activating GABA_ARs – iontophoresis, puffing, or uncaging. We initially chose iontophoresis for practical reasons, as it can be accomplished on a fairly standard slice recording rig, whereas uncaging requires the use of a 2-photon microscope due to the overlap of the activation spectra of caged compounds and PTLs²⁵. A drawback of iontophoresis is that it applies GABA in a gaussian concentration profile where the GABA concentration is lowest at the edge of the spot^{119,120}. Any unblocked LiGABARs from outside of the spot must first traverse the edge of the spot, where receptor activation will be lowest. Therefore, it is likely that using iontophoresis underestimates the actual exchange of LiGABARs in the spot region. However, in light of modeling results (Figure S6), it is likely that iontophoresis was the optimal method for us, regardless of equipment availability. GABA puffing with pressure produces similar spatial scales as iontophoresis, but with a slower time scale; we did not attempt it, but it should be as viable a method as iontophoresis.

Always, CREAP will yield the largest recovery when done on the smallest spatial scale and the longest time scale. The smallest size of iontophoresis that we could reliably and fully control with a similarly-size light spot was 20 μm (Figure 1D), though sizes as small as 10 μm were possible with a declining success rate. Due to the exponential nature of recovery (the $\alpha 1$ PhoRM recovery time constant was $\tau = 149$ s), extending whole cell patch clamp experiments beyond 15 minutes yields diminishing returns.

GABA uncaging could theoretically be a better option than iontophoresis since the uncaged GABA concentration would be more uniform across the spot and more spatially defined than iontophoresis. We assessed CREAP with uncaging of RuBi-GABA but did not find it to be a better option due to the low quantum yield and inherent antagonism of GABA_ARs that many such cages produce. Modeling suggests that we should expect at most ~50% recovery at this spot size (Figure S6) in the $\alpha 1$ PhoRM. Due to the much smaller currents elicited by RuBi-GABA compared to iontophoresis, the change in absolute current due to recovery would actually be much smaller with uncaging and difficult to detect (< 5pA). Given these parameters and the cost and complexity of using 2-photon microscopes and caged compounds, iontophoresis was far more practical in our hands, but future improved caged compounds such as “cloaked” GABA¹²¹ could produce more sensitive recoveries.

These technical constraints meant that the slowest average diffusion rate that we could detect with CREAP using iontophoresis was likely $\sim 0.001 \mu\text{m}^2/\text{s}$ (Figure 5F), which is still an order of magnitude faster than estimated average synaptic rates from the synapse model (Figure S5) and the slowest reported quantum dot-labeled GABA_ARs that were not considered ‘immobile’. For comparison, we estimated the $\alpha 1$ PhoRM average diffusion rate as $\sim 0.05 - 0.075 \mu\text{m}^2/\text{s}$ and the $\alpha 1$ and $\alpha 5$ overexpression rates as $\sim 0.0005 \mu\text{m}^2/\text{s}$. Thus, it is likely that diffusion of synaptic receptors was too slow for us to detect with CREAP, but we were able to detect the movement of extrasynaptic receptors and perhaps a population of fluid perisynaptic receptors.

Activity-dependence and cytoskeletal tethering of GABA_ARs

We set out to test the activity dependence of GABA_ARs by briefly applying a high concentration of NMDA to our slices, a strong treatment that evokes excitatory LTP (Figure S1), concurrent inhibitory LTD and an increase in GABA_AR mobility^{34,64}. Instead we saw a small but statistically non-significant decrease of mobility in the $\alpha 1$ PhoRM mouse, and no effect with overexpression conditions. This might be explained by the time course of the experiment: accompanying such a strong treatment was a slow expansion of slice tissue that prevented stable iontophoresis pipette placement relative to the dendrite for the first 20-30 minutes after the treatment, and any major changes as a result of treatment may have already come to equilibrium by the time recovery was measured. We never saw change of photo-inhibition over the course of CREAP, but in cells overexpressing $\alpha 1$ -LiGABAR we saw a significant decrease of photo-inhibition after treatment, whereas in the $\alpha 1$ PhoRM mouse we saw a slight increase. It is possible that any receptors mobilized by NMDA had become internalized^{51,69}, which could explain both the reduction of mobility with $\alpha 1$ PhoRM and reduction of photo-inhibition with $\alpha 1$ overexpression.

GABA_ARs are often tethered to actin^{39,48,105-107} and tubulin^{39,109,110} via intermediary proteins including gephyrin⁴⁰. $\alpha 5$ LiGABARs’ strong dependence on microtubules and not on actin for tethering was interesting, considering that it is known to interact with actin via radixin. The effects of actin polymerization on gephyrin are subtler than with tubulin³⁹, so this could be evidence of strong association with gephyrin. Also of note was how actin depolymerization counterintuitively caused a decrease of mobility in the $\alpha 1$ PhoRM mouse, a result that was not seen with overexpression.

Perhaps a surprising result was the observation that ablating gephyrin from the neurons did not increase the mobility of the $\alpha 1$ LiGABAR in the PhoRM mouse, since it is necessary for maintenance of inhibitory post-synapse density³² and IPSCs. However, gephyrin-independent synaptic clustering of $\alpha 1$ receptors in particular has been reported^{38,122}.

Implications and interpretations of the diffusion models

One important aspect of the models to consider, especially in light of reported single particle tracking experiments, is the difference between the average diffusion rate and the distributions of rates. In short, various combinations of diffusion rate distributions can lead to the same average diffusion rate, while resulting in very different degrees of CREAP recovery. These distributions are reflected in the time course of recovery, with biases towards faster receptors leading to a faster time constant. Our model's best estimate of the $\alpha 1$ PhoRM recovery results is with a high proportion of receptors on the faster end of the spectrum and very few immobile receptors. In contrast, we were not able to fit the time course of recovery for the overexpression experiments, so it's possible that the $3.81 \pm 1.78\%$ and $1.85 \pm 1.41\%$ recoveries we observed for $\alpha 1$ and $\alpha 5$ could be achieved by a broad distribution of slow rates; or, alternately, by an overwhelmingly immobile population of receptors supplemented by a relatively small fraction of very quickly moving extrasynaptic receptors. We attempted to address this question in Figure 5C-E and conclude that even if recovery is due entirely to extrasynaptic receptor diffusion, the extrasynaptic density of LiGABARs must be exceedingly small.

The synaptic diffusion model lends insights concerning the local environment in the dendrite by predicting that stretches of dendrite with more synapses can maintain those synaptic densities at a higher average diffusion rate (Figure S5C and D). This is simply because as synapses become more numerous and take up a larger fraction of the membrane, extrasynaptic receptors are more likely to run into them in their random walks. Likewise, faster-moving extrasynaptic receptors will be more likely to hit the synapse (Figure S5E). This has implications for local environments with high synaptic density, especially the soma and the proximal segment of the apical dendrite of CA1 pyramidal cells¹¹⁶ where we performed CREAP. It may also play a role in synaptic GABA_AR turnover and recycling by allowing faster flow of receptors in and out of the synapse.

The role of the $\alpha 1$ GABA_AR in hippocampal CA1 pyramidal cells

Pyramidal cells (PCs) of the CA1 region of the hippocampus predominantly express the $\alpha 1$, $\alpha 2$, and $\alpha 5$ isoforms¹²³⁻¹²⁵. Our experiments with the $\alpha 5$ PhoRM revealed that $\alpha 5$ contributes very little to CA1 PC synapses in normal conditions, and then only in the most distal dendrites in the lacunosum moleculare layer of CA1 (Figure S3). In the $\alpha 1$ PhoRM, we see 29% photoinhibition of electrically-evoked perisomatic currents, and slightly lower in the apical and basal dendrites. Considering that the $\alpha 1$ LiGABAR can be photo-inhibited by up to 78% when it is the only α subunit expressed and has both attached PTLs, $\alpha 1$ GABA_ARs may constitute as little as 38% of synaptic receptors, presumably leaving $\alpha 2$ as the remainder. One important unanswered question is the level of photoinhibition of LiGABARs with only a single PTL attached, whether through incomplete PTL labeling or by receptors containing two different α subunits. Although we cannot put a precise ceiling on the $\alpha 1$ GABA_AR contribution, we believe it is likely that $\alpha 1$ contributes to less than half of the GABAergic response at perisomatic synapses of CA1 pyramidal cells.

The situation changes markedly with viral overexpression and gives us a few valuable insights. Firstly, it should be noted that viral overexpression of an α subunit did not cause a change in the total inhibition measured as an E/I ratio²⁵ (although the kinetics may have been altered in the case of $\alpha 5$). The complete GABA_AR must still be composed with β and γ subunits limited to provision by the infected cell, so it is likely that the virally overexpressed LiGABARs competed out the native subunits. The average perisomatic electrically-evoked IPSC photo-inhibition in this condition is 46% (Fig 3C), which means that $\alpha 1$ LiGABARs contribute to at least 60% of synaptic

receptors. When applying GABA to a length of dendrite with iontophoresis, the photoinhibition rises from 13% in the $\alpha 1$ PhoRM to 33% with overexpression (Figure S2). Along with this comes a significant drop in the apparent mobility of overexpressed $\alpha 1$ LiGABARs to a level below the CREAP detection threshold, a recovery that was actually less in total magnitude than for $\alpha 1$ PhoRM, even considering the increased photo-inhibition. Overexpression therefore caused a large fraction of the $\alpha 1$ LiGABARs (and $\alpha 5$ as well) to accumulate at high-affinity synaptic sites and thereby decrease their average apparent diffusion rate.

There is substantial support in the literature for differential regulation of $\alpha 1$ and $\alpha 2$ GABA_ARs^{34,38,122,126–128}. $\alpha 2$ -containing receptors are preferentially localized to axo-axonic synapses in CA1 pyramidal cells, whereas $\alpha 1$ is associated with basket cell inputs to the soma. $\alpha 2$ -containing receptors are often expressed in combination with the $\beta 3$ and $\gamma 2$ subunits and associate very strongly with gephyrin. In fact, knocking out $\alpha 2$ from the genome leads to complete loss of gephyrin and synaptic clusters at axo-axonic inputs while having relatively little effect on basket cell inputs onto $\alpha 1\beta 2\gamma 2$ GABA_ARs³⁸. Thus, there is reasonable support for the idea that $\alpha 1$ and $\alpha 2$ operate at different locations under a different set of interacting proteins and plasticity rules, with $\alpha 2$ playing a more traditional synaptic role and $\alpha 1$ acting as a more fluid and promiscuous GABA_AR.

Our interpretation of the overexpression results is that there are multiple populations of GABA_ARs with very different diffusion rates. This hypothesis is supported by the many single particle tracking experiments with quantum dots, where a range of diffusion rates over 5 orders of magnitude is reported, from 0.00001 $\mu\text{m}^2/\text{s}$ to more than 0.1 $\mu\text{m}^2/\text{s}$, as well as reports of ‘immobile’ fractions as high as 0.5. In fact, our model required an immobile fraction of more than 0.8, reflecting an average diffusion rate of less than 0.0005 $\mu\text{m}^2/\text{s}$, to achieve the weak CREAP recovery seen in overexpression of $\alpha 1$ and $\alpha 5$ LiGABARs. In light of this interpretation, our data indicates that the $\alpha 1$ GABA_AR is normally a very mobile population of receptors and does not constitute the ‘core’ synaptic GABA_ARs that locked into place over much longer periods of time. Despite their relatively high mobility, these $\alpha 1$ GABA_ARs are nevertheless present at the synapse, as seen by inhibition of electrically-evoked IPSCs. This shouldn’t be a surprising result considering that recent reviews of GABA_AR lateral diffusion, plasticity, and trafficking paint a picture of a very dynamic inhibitory post-synapse able to rapidly adjust its size and strength through the recruitment and shedding of receptors, and where the $\alpha 1$ GABA_AR in particular seems to be less connected to the inhibitory post-synapse via gephyrin compared to $\alpha 2$. In the minute-to-minute and micron-to-micron shaping of synaptic signals, the $\alpha 1$ GABA_AR may play a particularly active role.

Acknowledgments

We thank the Arnold lab of USC for the kind gift of the gephyrin-ablating intrabody AAV-GFE3 virus. We also thank Dr. Mei Li (University of California, Berkeley) for preparing the viruses, and Neil Wilson Charlotte Taylor preparing the viral constructs.

The authors declare no competing interests.

Methods and Materials

The photoswitch compounds were synthesized as trifluoroacetate salts. The compounds were prepared as concentrated stocks (10–100 mM in anhydrous DMSO) and diluted in buffers for

receptor conjugation (final DMSO concentration <1% v/v). AAV9 (10^{13} to 10^{14} vg/ml; viral genomes/ml) encoding a mutant α subunit ($\alpha 1T125C$ or $\alpha 5E125C$), an eGFP marker, and a human synapsin-1 promoter was prepared by the UC Berkeley Gene Delivery Module following previously published procedures¹⁰⁴. The $\alpha 1$ -GABA_A and $\alpha 5$ -GABA_A PhoRM mice were generated by the UC Davis Mouse Biology program. All experiments were performed in accordance with the guidelines and regulations of the Animal Care and Use Committee at the University of California, Berkeley. Group data are reported as mean \pm SEM.

Unless otherwise indicated, chemicals and buffers were obtained from Sigma, Tocris, or Thermo-Fisher Scientific. All experiments were performed in accordance to the guidelines and regulations of the ACUC at the University of California, Berkeley.

Cloning and Virus Preparation. For neuronal expression, bi-cistronic pAAV constructs encoding a mutant α -subunit ($\alpha 1T125C$ or $\alpha 5E125C$) and an eGFP marker were prepared following the previously published procedures¹⁰⁴. Each mutant α -subunit has an N-terminal *myc* epitope tag which does not affect receptor function and synaptic targeting^{33,129}. Gene expression is conferred by a human synapsin-1 promoter¹³⁰. AAV-flex-ReaChR-citrine DNA was obtained from Addgene (catalog #50955). The DNA clones were subsequently packaged into AAV9 at a titer of 10^{12} – 10^{14} vg/mL.

Animals. Pregnant wildtype female mice for neonatal viral injection (see below) were obtained from Jackson Laboratories (JAX). $\alpha 1T125C$ and $\alpha 5E125C$ knock-in mice ($\alpha 1$ and $\alpha 5$ GABA_AR PhoRM) were generated as described in²⁵. SOM-cre $\alpha 5$ -GABA_AR PhoRM mice were derived from crossing $\alpha 5$ -GABA_AR PhoRM and *Sst*^{tm2.1(cre)Zjh/J} (Jackson lab stock # 013044).

Viral Expression of Mutant α -Subunits and ReaChR in the Mouse Hippocampus. Neonates (P0–P3) of wild-type mice were anesthetized on ice, placed in a custom mold, and injected with 10–30 nL of virus bilaterally in the hippocampus (0.6–0.8 mm lateral to lambda, 0.6–0.9 mm anterior, 0.8–1 mm ventral). Experiments were carried out 2–3 weeks after injection.

Preparation of Acute Brain Slices. Mice (2–3 weeks old) of both sexes were used for slice preparation. Acute brain slices (350 μ m) of hippocampus were prepared in ice-cold cutting solution containing (in mM): 85 NaCl, 2.5 KCl, 0.5 CaCl₂, 4 MgCl₂, 1.25 NaH₂PO₄, 25 NaHCO₃, 75 sucrose, 0.5 ascorbic acid and 25 glucose (saturated with 95% O₂ and 5% CO₂; pH 7.4). After sectioning, slices were transferred to a holding chamber containing artificial cerebrospinal fluid (aCSF) containing (in mM): 126 NaCl, 2.5 KCl, 2.5 CaCl₂, 1.3 MgCl₂, 1.25 NaH₂PO₄, 26 NaHCO₃, and 10 glucose (saturated with 95% O₂ and 5% CO₂; pH 7.4) at 34 °C for 20 min and were then cooled down to room temperature. PTL treatment was carried out at room temperature (see below).

Ex vivo PTL Treatment. Slices (in aCSF) were treated with TCEP (5 mM, 5 min), washed, and incubated with either PAG-1C or PAG-1C-G1 (25–50 μ M, with 500 μ M guanidinium hydrochloride) for 40–60 min at room temperature.

IPSC recordings in hippocampal neurons. Slices were placed in a recording chamber on an upright moving-stage microscope (Slicescope, Scientifica UK) with Dodt contrast IR optics and

GFP and RFP epifluorescence. Slices were perfused with aCSF warmed to 34° C with an in-line heater (Thermoclamp-1, AutoMate Scientific) at 1–2 mL/min. Whole-cell recordings were made from (GFP-positive for viral overexpression experiments) CA1 pyramidal cells with glass microelectrodes ($R = 3\text{--}6\text{ M}\Omega$) filled with internal solution containing (in mM): 108 Cs-gluconate, 2.8 NaCl, 20 HEPES, 5 TEA-Cl, 0.4 EGTA, 4 Mg-ATP, 0.3 Na-GTP and 10 phosphocreatine, adjusted to ~ 7.25 pH and ~ 290 mOsm. To record isolated IPSCs, 3 mM kynurenic acid was added to the aCSF and cells were held at the reversal potential of excitatory inputs (0 mV). A glass stimulating electrode (filled with aCSF) was placed in stratum pyramidale $\sim 100\ \mu\text{m}$ away from the recorded cell. Synaptic responses were evoked by a 0.2-ms, 10–100 μA current pulse delivered via a stimulus isolation unit (AMPI). Conditioning light (385 nm and 500 nm for PAG-1C or 460 nm for PAG-1C-G1) was generated by an LED light source (pE-4000, CoolLED) and delivered through a digital multimirror display (CEL5500, Digital Light Innovations) to the microscope objective through a set of lenses (Thor Labs) calculated to backfill the objective and minimize chromatic aberration. Light intensity at the objective was (in mW/mm^2): 3.46 at 385 nm, 7.54 at 460nm, 3.76 at 625 nm. Membrane currents were amplified (Axopatch 500B; Molecular Devices), digitized (Digidata 1550A; Molecular Devices) and recorded (pClamp 10; Molecular Devices) to a desktop computer.

GABA iontophoresis in hippocampal neurons. Whole-cell recordings from hippocampal neurons were performed as described above, except the intracellular solution was supplemented with 20–40 μM Alexa Fluor 594 and the aCSF was supplemented with 0.1 μM TTX. A glass iontophoresis pipette^{119,120} was filled with 5–10 mM GABA dissolved in water and pH adjusted to 5.0. The pipette tip was pierced into the slice and placed 1–2 μm from the apical dendrite $\sim 100\ \mu\text{m}$ from the soma. GABA was applied to the dendrite with a an iontophoresis box (Model 160 Micro-iontophoresis Programmer, WPI).

ReaChR-evoked IPSC recordings. Whole cell recordings from hippocampal neurons of $\alpha 5$ LiGABAR PhoRM x SOM-cre mice neonatally injected with FLEX-ReaChR were performed as described above. ReaChR was activated by 1–10 ms flashes of 625 nm LED light.

Current-clamp recordings in hippocampal neurons. Whole-cell recordings from hippocampal were performed using the instrumental setup described above. The internal solution contained (mM): 116 K-Gluconate, 6 KCl, 2 NaCl, 20 HEPES, 0.5 EGTA, 4 Mg-ATP, 0.3 Na-GTP and 10 phosphocreatine, adjusted to ~ 7.25 pH and ~ 290 mOsm.

Data Analysis. The electrophysiology data were analyzed in Clampfit 10 (Molecular Device) followed by customized routines in Matlab (Mathworks). CREAP iontophoresis peak data was linearly corrected for drift between the starting and end averages recorded in 385 nm light and normalized per cell as a fraction of the total photo-inhibited current. Recovery was calculated per cell as the mean current in the last 2 minutes of the 15-minute recovery period divided by the total photo-inhibited current measured in the 2 minutes following recovery. Recoveries of greater than 1 were considered 1 and recoveries less than 0 were considered 0. The mean recovery was tested for significance with a one-sample t-test against a mean of 0. Group data was compared using a one-way ANOVA.

Representative IPSC and iontophoresis traces shown in Figures 1-4 are the average from 3 or more individual traces. For curve fitting in Figure 2A, we performed single exponential fit $y = a \cdot \exp(b \cdot x)$ to derive the time and depth constants in Clampfit.

Statistics were performed using Microsoft Excel and Matlab.

Diffusion Models. Diffusions models were calculated in Matlab with Fick's second law of diffusion:

$$\frac{\partial \rho}{\partial t} = D \frac{\partial^2 \rho}{\partial x^2}$$

Where ρ is the density of GABA_ARs, t is time, D is the diffusion coefficient, and x is the position. A cell with a soma and a single apical dendrite was divided into segments of length x , and the change in density between adjacent segments was computed at time intervals of t . Photo-inhibition with a spot was simulated by reducing the GABA_AR density by the photo-inhibition rate in a defined region along the dendrite. Recovery was calculated as the number of GABA_ARs in the spot region at the last time point as a fraction of the difference between the full number of receptors (without a spot) and the initial number of receptors in the spot.

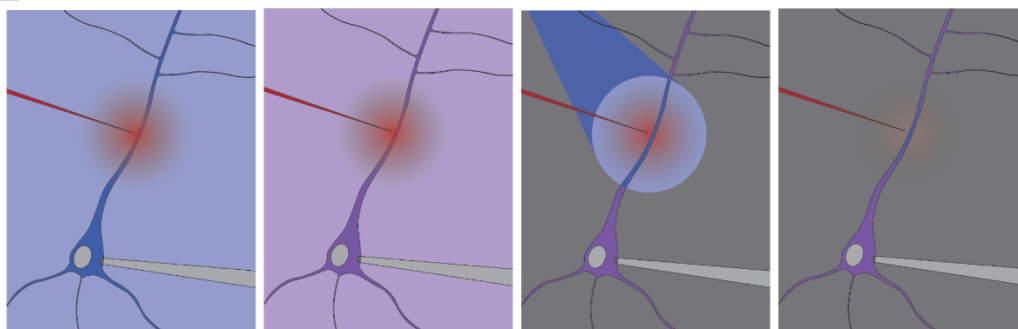
Diffusion rates of synaptic and extrasynaptic receptors were distributed into three groups estimated from the data presented primarily in²³ but other sources as well^{23,34,54,74,75}. The immobile fraction constituted a portion of the synaptic receptors only and had a diffusion rate of 0. The remaining synaptic receptors were distributed in the original proportions.

GABA_AR densities at synaptic and extrasynaptic sites were estimated from the literature^{54,59,116-118}.

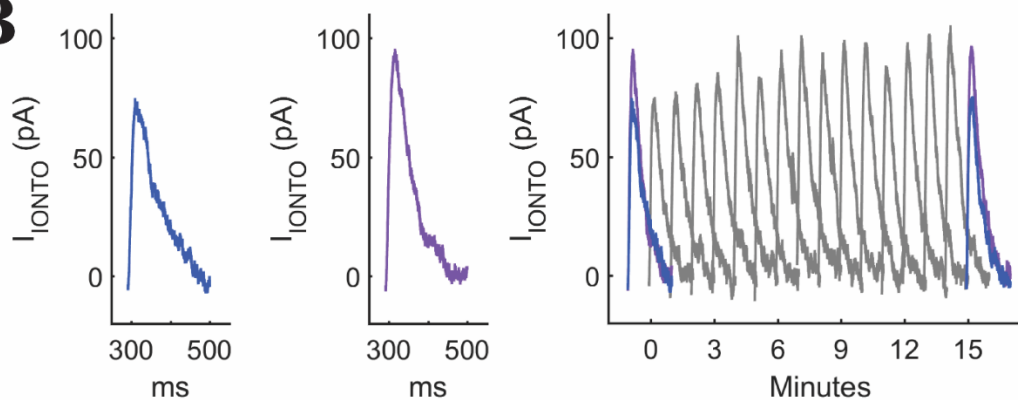
The synaptic diffusion model was calculated by defining a synaptic area and extrasynaptic area per given micron of dendrite, diffusion rates for both areas, and initial GABA_AR density for both areas. Fick's second law of diffusion was applied to each area to determine the flux of GABA_ARs, with flux from the extrasynaptic region limited by the ratio of the area of synaptic membrane to the area of extrasynaptic membrane. The total number of receptors was conserved, allowing receptors to move between regions to an equilibrium distribution.

Figures

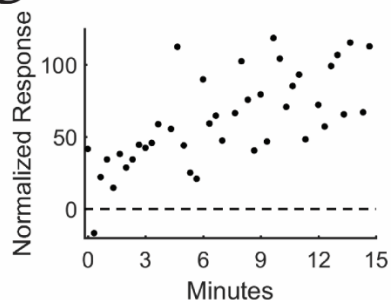
A



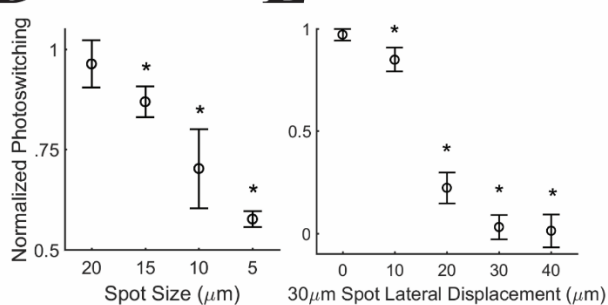
B



C



D



E

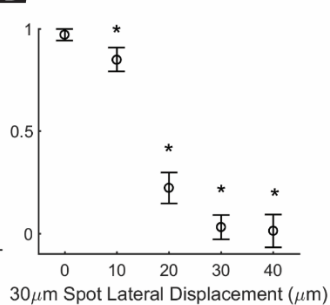


Figure 1. Measuring lateral diffusion of LiGABARs with electrophysiology: current recovery after photo-inhibition (CREAP) (A-B) In an acute brain slice, LiGABARs activated by iontophoresis of GABA were focally photo-inhibited and current is monitored for recovery. (A) LiGABARs can be inhibited with 460nm light (left) and disinhibited with 385nm light (left-center). By photo-inhibiting only the LiGABARs activated by iontophoresis (right-center), lateral diffusion of disinhibited receptors caused a rise in recorded current over time (right). (C) Example iontophoresis-evoked currents of CREAP in a hippocampal CA1 pyramidal cell. Recovery was measured at the last 2 minutes of the experiment as the percent of photo-inhibited current regained. (D) The spatial extent of iontophoresis-applied GABA was measured by shrinking the 460 nm spot. A 20 μm spot allowed full photo-inhibition of iontophoresis currents. (E) The sharpness of the 460 nm spot was demonstrated by translating the spot orthogonally to the dendrite. As the spot was moved off the dendrite, photo-inhibition was lost.

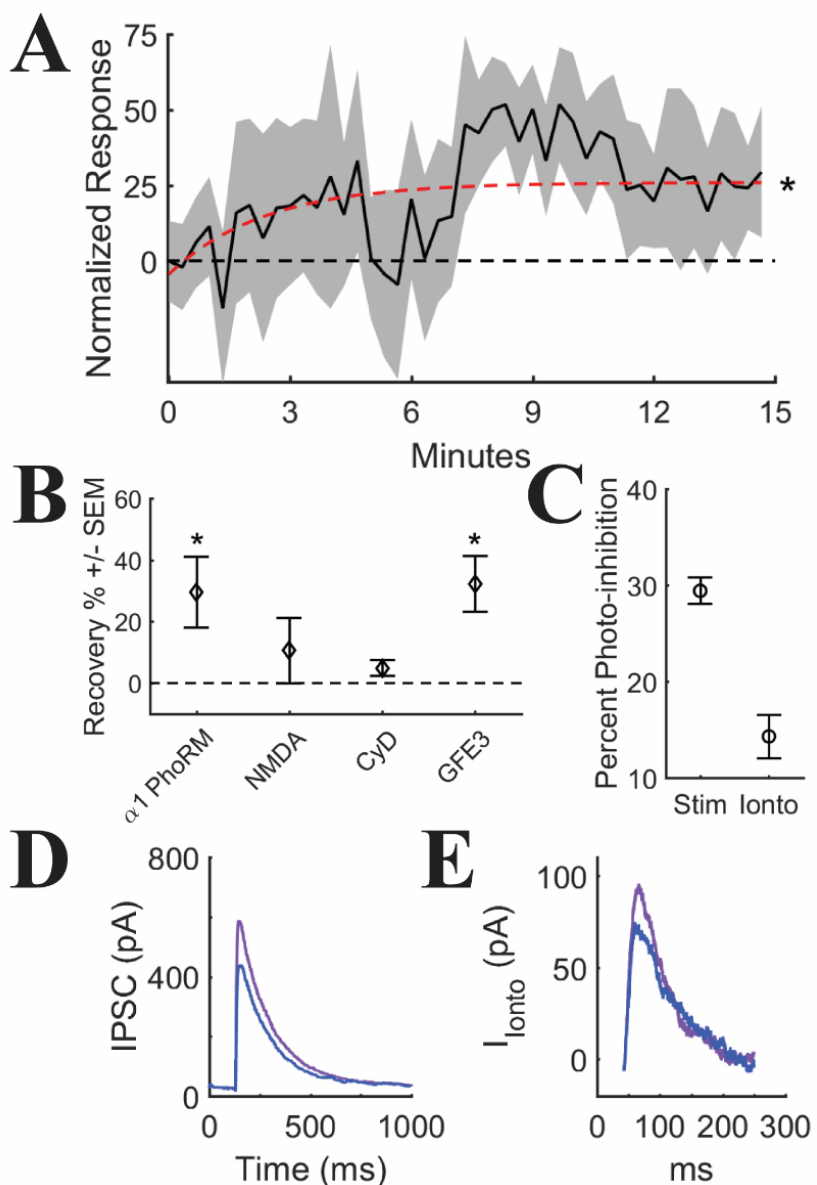


Figure 2. Lateral diffusion in the $\alpha 1$ -LiGABAR Photoswitch-Ready Mouse (PhoRM) (A) Significant $29.5 \pm 11.5\%$ recovery of iontophoresis current over a 15-minute period ($p = 0.036$, t-test, $n = 8$, plotted as mean \pm SEM denoted by gray region) (B) $\alpha 1$ PhoRM group recovery data for all tested conditions, given as mean \pm SEM. NMDA was briefly applied to the slice to cause eLTP/iLTD and no recovery was seen after treatment ($p = 0.423$, t-test, $n = 3$). Cytochalasin D (10 μM) was applied to the slice for 2 h to disrupt actin polymerization; no recovery was seen after treatment ($p = 0.105$, t-test, $n = 8$). An adeno-associated virus encoding a gephyrin-ablating intrabody (GFE3) was injected into the $\alpha 1$ PhoRM mouse and recovery was recorded from infected cells ($p = 0.017$, t-test, $n = 6$) that was not different from the control condition ($p = 0.099$, one-way ANOVA). (C) Maximal photo-inhibition of iontophoresis-evoked GABA currents ($12.72 \pm 2.54\%$, $n = 8$), and perisomatic electrically-evoked GABA currents ($29.41 \pm 1.37\%$, $n = 8$). (D) Example of perisomatic electrically-evoked IPSC photo-inhibition. (E) Example of iontophoresis-evoked current photo-inhibition.

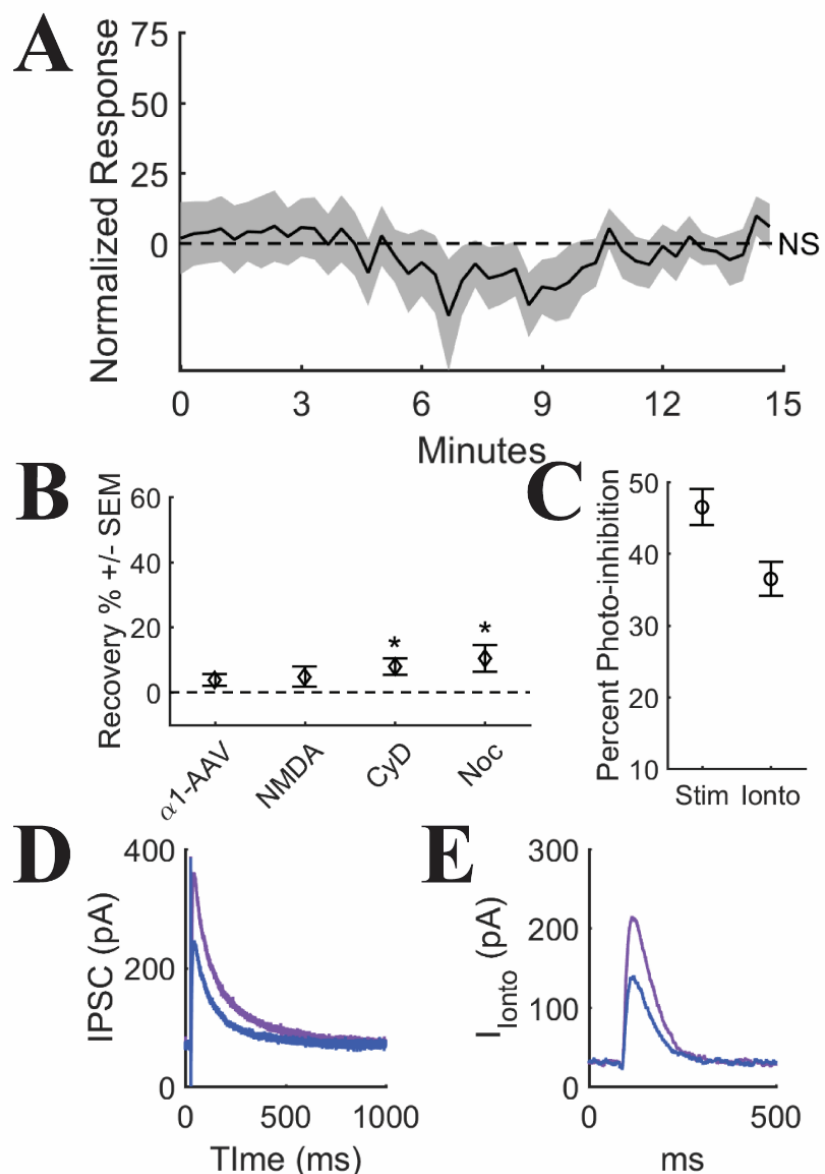


Figure 3. Lateral diffusion in the wildtype mouse injected with AAV- $\alpha 1$ -LiGABAR (A) No recovery was observed with overexpressed $\alpha 1$ LiGABAR ($p = 0.065$, t-test, $n = 9$, plotted as mean \pm SEM denoted by gray region) (B) AAV- $\alpha 1$ group recovery data for all tested conditions, given as mean \pm SEM. No recovery was seen in slices treated with NMDA ($p = 0.177$, t-test, $n = 6$). A $7.97 \pm 2.53\%$ recovery was seen in slices treated with cytochalasin D ($p = 0.009$, t-test, $n = 12$). Nocodazole ($10 \mu\text{M}$) was applied to the slices for 2 h before recording recovery of $10.36 \pm 4.14\%$ ($p = 0.031$, t-test, $n = 7$). No treatments were significantly different from control ($p = 0.362$, one-way ANOVA). (C) Maximal photo-inhibition of iontophoresis-evoked GABA currents ($32.81 \pm 4.22\%$, $n = 9$) and of perisomatic electrically-evoked IPSCs ($46.48\% \pm 2.51\%$, $n = 5$). (D) Example of perisomatic electrically-evoked IPSC photo-inhibition. (E) Example of iontophoresis-evoked current photo-inhibition.

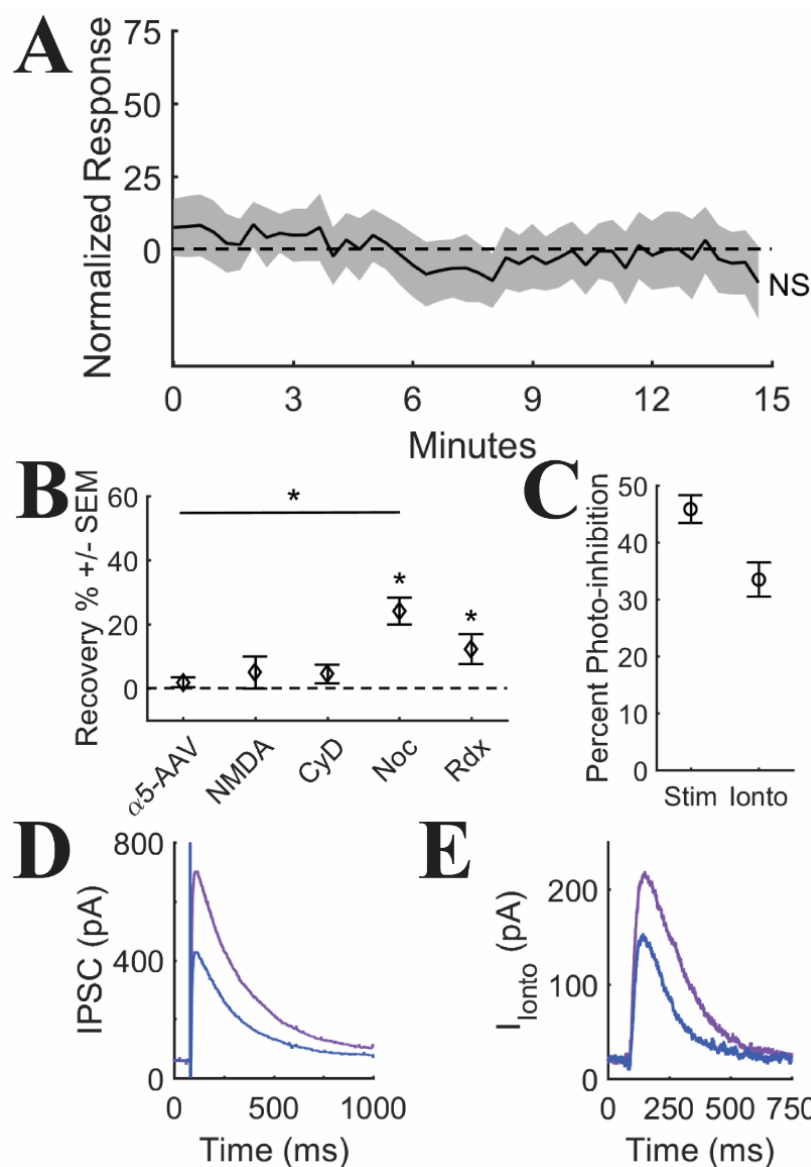


Figure 4. Lateral diffusion in the wildtype mouse injected with AAV- $\alpha 5$ -LiGABAR (A) No recovery was observed with overexpressed $\alpha 5$ LiGABAR ($p = 0.225$, t-test, $n = 9$, plotted as mean \pm SEM denoted by gray region) (B) AAV- $\alpha 5$ group recovery data for all tested conditions, given as mean \pm SEM. No recovery was seen in slices treated with NMDA ($p = 0.5$, t-test, $n = 2$). Recovery was not seen in slices treated with cytochalasin D ($p = 0.194$, t-test, $n = 5$). Recovery of $24.1 \pm 4.4\%$ was seen when nocodazole was applied to the slices ($p = 0.001$, t-test, $n = 7$) which was significantly different to control ($p = 0.0004$, one-way ANOVA). An adeno-associated virus encoding dominant-negative radixin mutant T564A was co-injected with AAV- $\alpha 5$ -LiGABAR into wildtype mice and $12.2 \pm 4.6\%$ recovery was recorded in infected cells ($p = 0.047$, t-test, $n = 6$). (C) Maximal photo-inhibition of iontophoresis-evoked GABA currents ($38.45 \pm 2.14\%$, $n = 29$) and perisomatic electrically-evoked IPSCs ($45.83 \pm 2.44\%$, $n = 8$). (D) Example of perisomatic electrically-evoked IPSC photo-inhibition. (E) Example of iontophoresis-evoked current photo-inhibition.

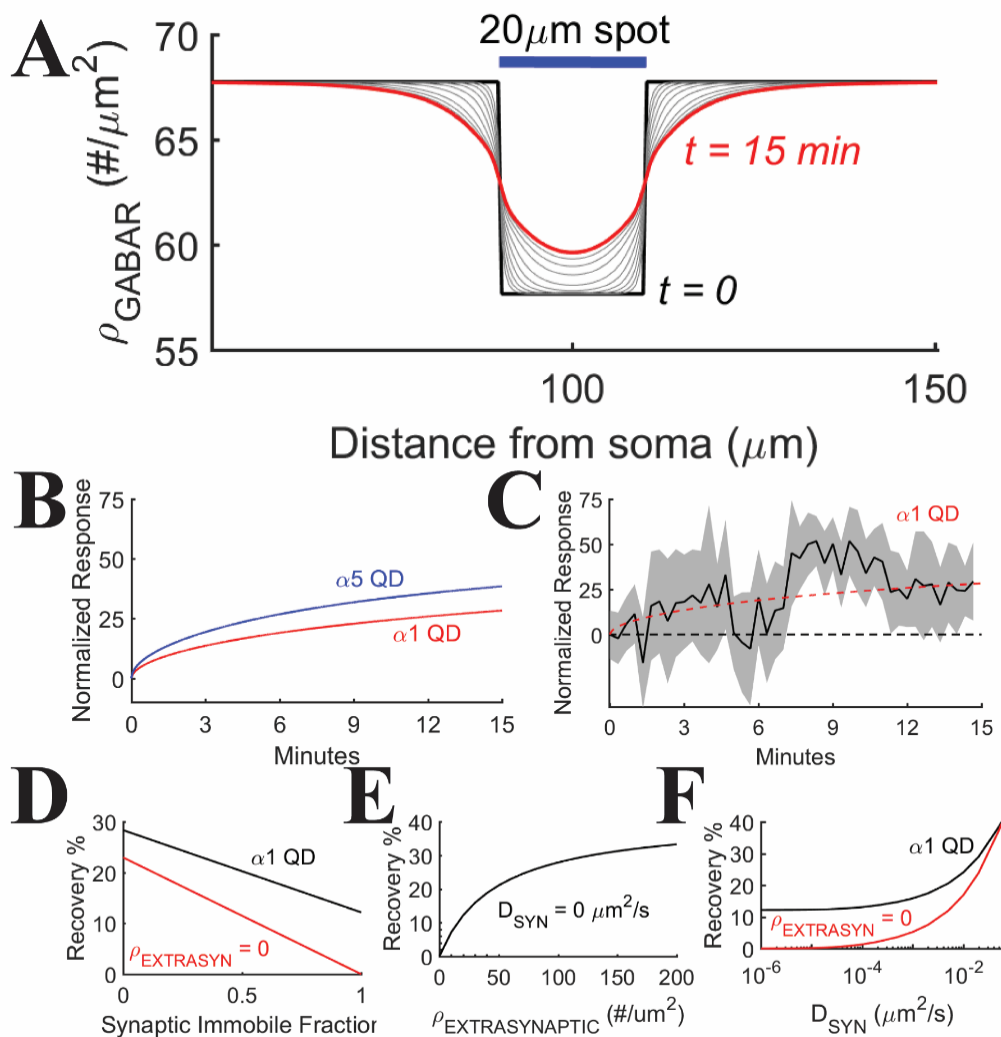


Figure 5. A mathematical model of CREAP applying Fick's laws of diffusion. (A) Simulation of LiGABAR density along the 250 μm -long apical dendrite of a neuron. At time 0, a 20 μm spot of $\alpha 1$ -LiGABARs at a point 100 μm from the soma was photo-inhibited by reducing the density of GABA_ARs (black line). Over 15 minutes, lateral diffusion causes mixing of receptors (grey lines showing increasing time intervals). Recovery is calculated as the percent of density within the spot at 15 minutes (red line) compared to no photo-inhibition. (B) Predicted recovery of a 20 μm spot using diffusion rate and distribution data from quantum dot single particle tracking experiments. The $\alpha 1$ GABA_AR simulated recovery is 28.3% with a time constant $\tau = 196$ s and average synaptic diffusion rate $D_{\text{SYN}} = 0.027 \mu\text{m}^2/\text{s}$; the $\alpha 5$ GABA_AR recovery is 38.4% with $\tau = 178$ s and $D_{\text{SYN}} = 0.072 \mu\text{m}^2/\text{s}$. (C) Simulated recovery of $\alpha 1$ GABA_AR compared to actual data from $\alpha 1$ LiGABAR PhoRM experiments. (D) Simulated recovery of $\alpha 1$ as a fraction of synaptic receptors that are immobilized, depicting $\alpha 1$ QD data (black) and the same data calculated with the density of extrasynaptic receptors set to zero (red). (E) Predicted recovery as a function of extrasynaptic receptor density (F) Predicted recovery as a function of a single average synaptic diffusion rate D_{SYN} , with (black) or without (red) extrasynaptic LiGABARs.

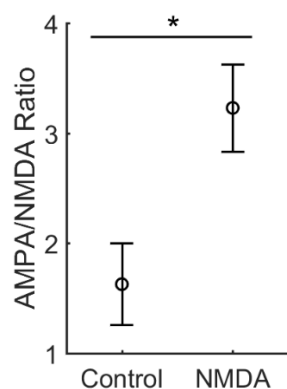
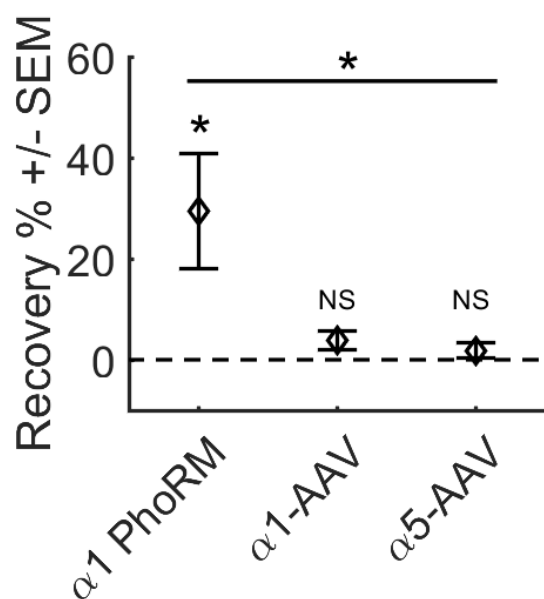


Figure S1. Treatment with NMDA (50 μ M) and glycine (5 μ M) causes LTP as measured by AMPA/NMDA ratios. AMPAR currents were measured at the peak with the cell held at -70 mV; NMDAR currents were measured 60-80 ms after stimulation while holding the cell at +40 mV. AMPA/NMDA ratio was determined in control slices and compared to the ratio in slices that were treated for 2-3 minutes. Treatment caused a significant increase in the AMPA/NMDA ratio from 1.63 ± 0.37 to 3.23 ± 0.40 ($p = 0.009$, two-tailed t-test, $n = 7$ and 12 , respectively).

A



B

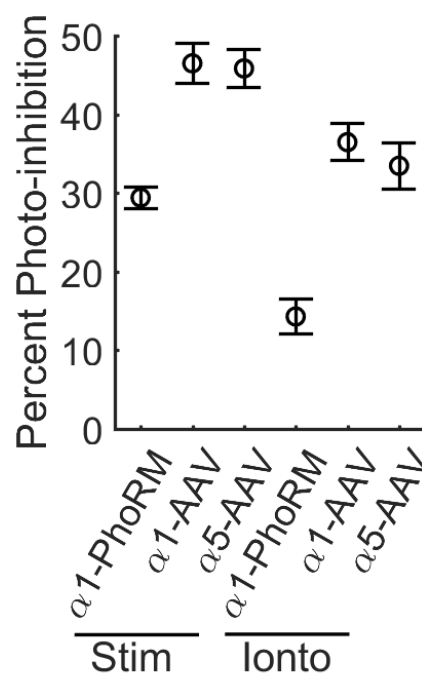


Figure S2. (A) Comparison of CREAP recovery between $\alpha 1$ PhoRM and viral overexpression of $\alpha 1$ or $\alpha 5$. The $\alpha 1$ PhoRM showed a significant recovery of 29.5 ± 11.5 ($p = 0.036$, t-test, $n = 8$), and was a significantly different result compared to overexpression conditions ($p = 0.009$, one-way ANOVA). (B) Comparison of maximal photo-inhibition of perisomatic electrical stimulation evoked IPSCs (Stim) and GABA iontophoresis evoked currents (Ionto).

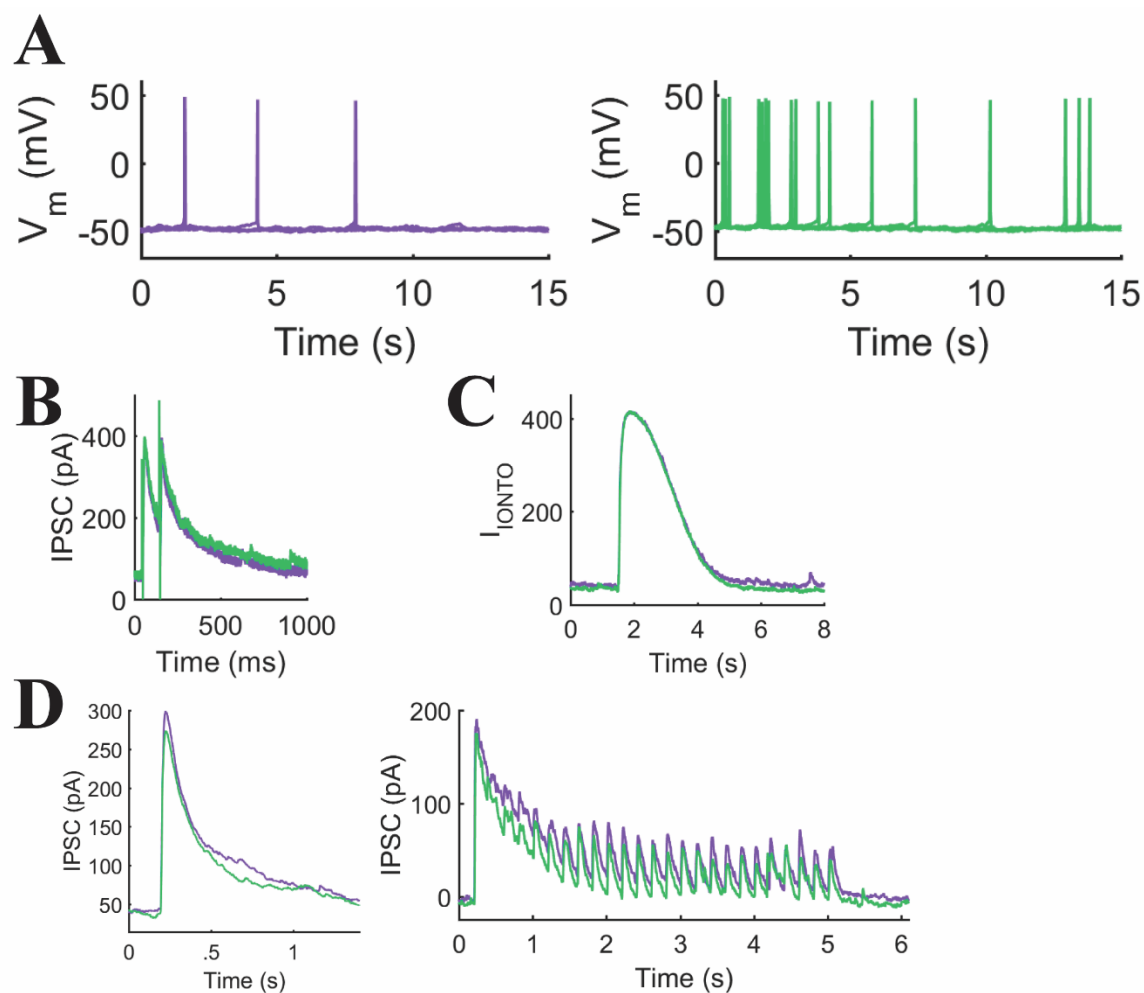


Figure S3. Observations from the $\alpha 5$ -LiGABAR PhoRM mouse. (A) Photo-modulation of membrane potential and spiking of hippocampal CA1 pyramidal cells. (B) No photo-inhibition of perisomatic electrically-evoked IPSCs. (C) No photo-inhibition of iontophoresis-evoked GABA currents. (D) Photo-inhibition of IPSCs evoked by ReaChR expressed in SOM⁺ interneurons. (Left) Weak photo-inhibition ($6.54 \pm 1.68\%$, $n = 7$) of IPSCs evoked by brief (~ 12 ms) flashes of 635 nm light. (Right) Example of greater photo-inhibition (32.19%) observed over trains of flashes (5 Hz) compared to the first peak (7.77%).

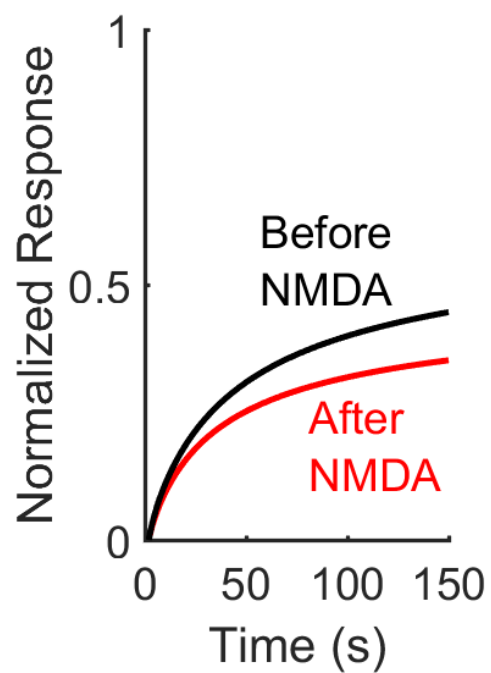


Figure S4. Recreation of FRAP data using a GABA_AR diffusion model. Compare to Figure 9F from (Petrini 2014)⁵⁴. Model parameters: spot size 0.5 μm ; immobile fraction 0.3 before NMDA, 0.45 after; diffusion rates listed in Table S2.

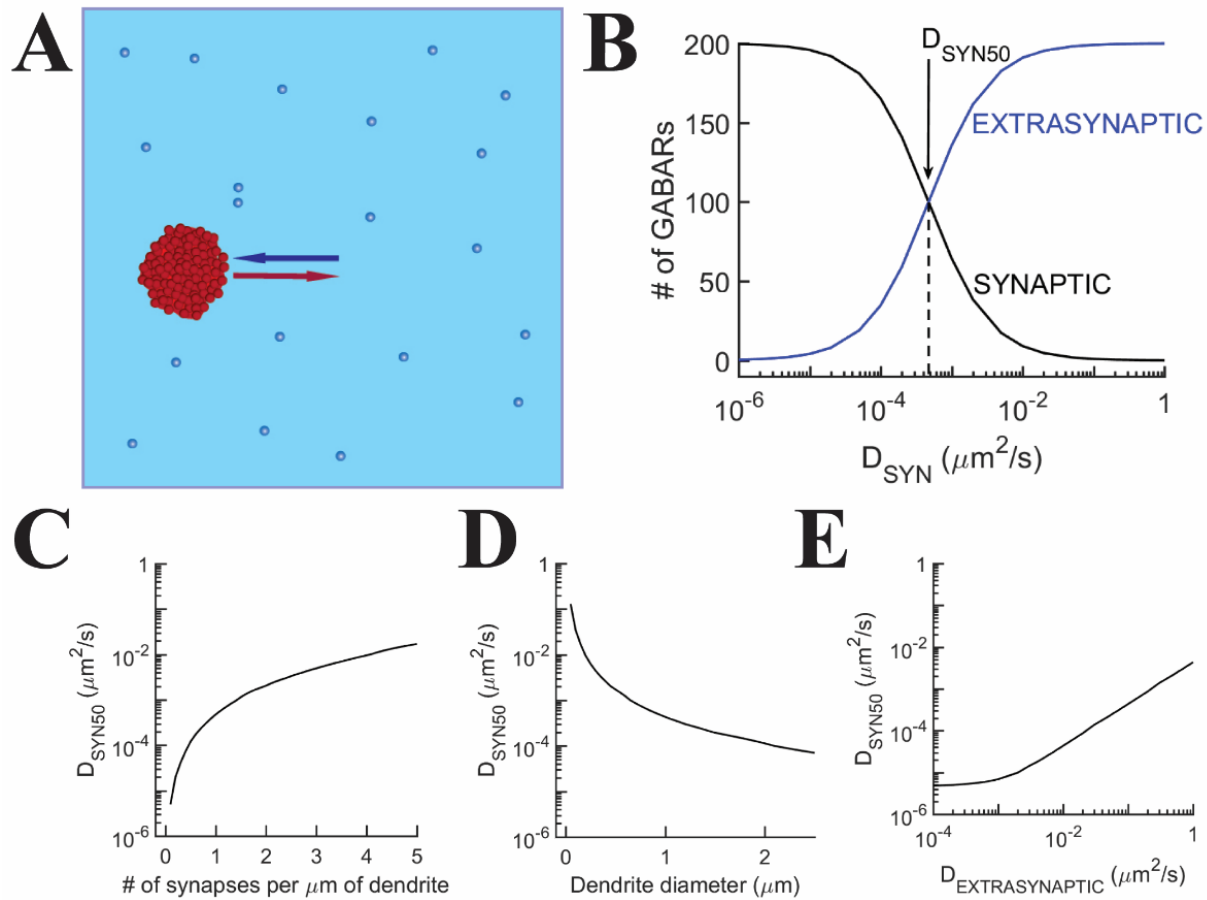


Figure S5. A simple diffusion model of inhibitory synapses. (A) A representative segment of dendrite with synaptic and extrasynaptic zones with different areas and diffusion rates. The total number of receptors is conserved and initially begins in the synaptic zone. Over time the receptors are redistributed to equilibrium between the two zones. (B) The equilibrium distribution is calculated over a range of synaptic diffusion rates D_{SYN} . The D_{SYN} at which the synapse maintains half of its original receptors is noted as D_{SYN50} , estimated at $\sim 0.0005 \mu\text{m}^2/\text{s}$ in a typical dendrite. D_{SYN50} is calculated as a function of (C) synapse density along the dendrite, (D) dendrite diameter, and (E) the diffusion rate of extrasynaptic receptors. A larger D_{SYN50} indicates a more fluid synapse at equilibrium.

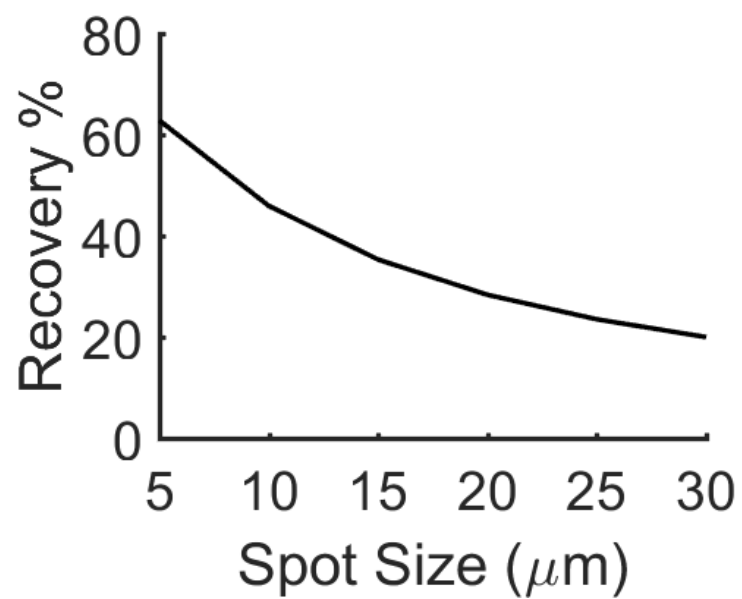


Figure S6. Simulation of CREAP with different spot sizes.

Table S1. Parameters used in dendrite lateral diffusion model.

Diffusion rates in $\mu\text{m}^2/\text{s}$ (fraction of total)	$\alpha 1$ QD	$\alpha 5$ QD
Synaptic Slow	0.0004 (.25)	0.0005 (.1)
Synaptic Med	0.0175 (.5)	0.0113 (.38)
Synaptic Fast	0.073 (.25)	0.13 (.52)
Extrasynaptic Slow	0.0052 (.2)	0.00095 (.13)
Extrasynaptic Med	0.04 (.4)	0.0475 (.37)
Extrasynaptic Fast	0.225 (.4)	0.2265 (.5)

Table S2. Parameters used in synapse diffusion model.

Initial synapse density ($\#/\mu\text{m}^2$)	1000
Initial synaptic number	200
Synapse size (μm^2)	0.2
Extrasynaptic diffusion rate ($\mu\text{m}^2/\text{s}$)	0.1
Dendrite diameter (μm)	1

Table S3. Parameters used in FRAP simulation.

Diffusion rates in $\mu\text{m}^2/\text{s}$ (fraction of total)	Before NMDA	After NMDA
Synaptic Slow	0.006 (.25)	0.00095 (.25)
Synaptic Med	0.0305 (.5)	0.015 (.5)
Synaptic Fast	0.1135 (.25)	0.034 (.25)
Extrasynaptic Slow	0.0052 (.2)	0.0052 (.2)
Extrasynaptic Med	0.04 (.4)	0.04 (.4)
Extrasynaptic Fast	0.225 (.4)	0.225 (.4)

References

1. Farrant, M. & Nusser, Z. Variations on an inhibitory theme: phasic and tonic activation of GABAA receptors. *Nat. Rev. Neurosci.* **6**, 215–229 (2005).
2. Higley, M. J. Localized GABAergic inhibition of dendritic Ca²⁺ signalling. *Nat. Rev. Neurosci.* **15**, 567–572 (2014).
3. Treiman, D. M. GABAergic Mechanisms in Epilepsy. *Epilepsia* **42**, 8–12 (2001).
4. Maćkowiak, M., Mordalska, P. & Wędzony, K. Neuroligins, synapse balance and neuropsychiatric disorders. *Pharmacol. Rep.* **66**, 830–835 (2014).
5. Wehr, M. & Zador, A. M. Balanced inhibition underlies tuning and sharpens spike timing in auditory cortex. *Nature* **426**, 442–446 (2003).
6. Rudolph, U. & Möhler, H. GABAA Receptor Subtypes. *Annu. Rev. Pharmacol. Toxicol.* **54**, 483–507 (2014).
7. Guidotti, A. *et al.* GABAergic dysfunction in schizophrenia: new treatment strategies on the horizon. *Psychopharmacology (Berl.)* **180**, 191–205 (2005).
8. Bateup, H. S. *et al.* Excitatory/inhibitory synaptic imbalance leads to hippocampal hyperexcitability in mouse models of Tuberous Sclerosis. *Neuron* **78**, 510–522 (2013).
9. Vithlani, M., Terunuma, M. & Moss, S. J. The Dynamic Modulation of GABA_A Receptor Trafficking and Its Role in Regulating the Plasticity of Inhibitory Synapses. *Physiol. Rev.* **91**, 1009–1022 (2011).
10. Mele, M., Leal, G. & Duarte, C. B. Role of GABA_A R trafficking in the plasticity of inhibitory synapses. *J. Neurochem.* **139**, 997–1018 (2016).
11. Olsen, R. W. & Sieghart, W. GABAA receptors: Subtypes provide diversity of function and pharmacology. *Neuropharmacology* **56**, 141–148 (2009).

12. Korpi, E. R., Gründer, G. & Lüddens, H. Drug interactions at GABAA receptors. *Prog. Neurobiol.* **67**, 113–159 (2002).
13. Fritschy, J.-M. & Mohler, H. GABAA-receptor heterogeneity in the adult rat brain: Differential regional and cellular distribution of seven major subunits. *J. Comp. Neurol.* **359**, 154–194 (1995).
14. Picton, A. J. & Fisher, J. L. Effect of the α subunit subtype on the macroscopic kinetic properties of recombinant GABAA receptors. *Brain Res.* **1165**, 40–49 (2007).
15. Wisden, W., Laurie, D. J., Monyer, H. & Seeburg, P. H. The Distribution of 13 GABA_A Receptor Subunit mRNAs in the Rat Brain. I. Telencephalon, Diencephalon, Mesencephalon. 23
16. SPERK, G., SCHWARZER, C., TSUNASHIMA, K., FUCHS, K. & SIEGHART, W. GABAA RECEPTOR SUBUNITS IN THE RAT HIPPOCAMPUS I: IMMUNOCYTOCHEMICAL DISTRIBUTION OF 13 SUBUNITS. 14
17. PIRKER, S., SCHWARZER, C., WIESELTHALER, A., SIEGHART, W. & SPERK, G. GABAA RECEPTORS: IMMUNOCYTOCHEMICAL DISTRIBUTION OF 13 SUBUNITS IN THE ADULT RAT BRAIN. 36
18. Mortensen, M., Patel, B. & Smart, T. G. GABA Potency at GABAA Receptors Found in Synaptic and Extrasynaptic Zones. *Front. Cell. Neurosci.* **6**, (2012).
19. Nusser, Z., Sieghart, W. & Somogyi, P. Segregation of Different GABAA Receptors to Synaptic and Extrasynaptic Membranes of Cerebellar Granule Cells. *J. Neurosci.* **18**, 1693–1703 (1998).
20. Serwanski, D. R. *et al.* Synaptic and nonsynaptic localization of GABAA receptors containing the $\alpha 5$ subunit in the rat brain. *J. Comp. Neurol.* **499**, 458–470 (2006).

21. Christie, S. B. $\alpha 5$ Subunit-containing GABAA receptors form clusters at GABAergic synapses in hippocampal cultures. 4
22. Loeblich, S., Bähring, R., Katsuno, T., Tsukita, S. & Kneussel, M. Activated radixin is essential for GABAA receptor $\alpha 5$ subunit anchoring at the actin cytoskeleton. *EMBO J.* **25**, 987–999 (2006).
23. Hausrat, T. J. *et al.* Radixin regulates synaptic GABAA receptor density and is essential for reversal learning and short-term memory. *Nat. Commun.* **6**, (2015).
24. Essrich, C., Lorez, M., Benson, J. A., Fritschy, J.-M. & Lüscher, B. Postsynaptic clustering of major GABAA receptor subtypes requires the $\gamma 2$ subunit and gephyrin. *Nat. Neurosci.* **1**, 563–571 (1998).
25. Lin, W.-C. *et al.* A Comprehensive Optogenetic Pharmacology Toolkit for In Vivo Control of GABA A Receptors and Synaptic Inhibition. *Neuron* **88**, 879–891 (2015).
26. Olsen, R. W. & Sieghart, W. International Union of Pharmacology. LXX. Subtypes of γ -Aminobutyric Acid A Receptors: Classification on the Basis of Subunit Composition, Pharmacology, and Function. Update. *Pharmacol. Rev.* **60**, 243–260 (2008).
27. SUR, C., QUIRK, K., DEWAR, D., ATACK, J. & MCKERNAN, R. Rat and Human Hippocampal $\alpha 5$ Subunit -Containing $\gamma 2$ -Aminobutyric Acid A Receptors Have $\alpha 5$ $\gamma 2$ Pharmacological Characteristics. 6
28. Thomas, P., Mortensen, M., Hosie, A. M. & Smart, T. G. Dynamic mobility of functional GABAA receptors at inhibitory synapses. *Nat. Neurosci.* **8**, 889–897 (2005).
29. Bogdanov, Y. *et al.* Synaptic GABAA receptors are directly recruited from their extrasynaptic counterparts. *EMBO J.* **25**, 4381–4389 (2006).

30. Petrini, E. M. & Barberis, A. Diffusion dynamics of synaptic molecules during inhibitory postsynaptic plasticity. *Front. Cell. Neurosci.* **8**, (2014).
31. Tretter, V. *et al.* Gephyrin, the enigmatic organizer at GABAergic synapses. *Front. Cell. Neurosci.* **6**, (2012).
32. Jacob, T. C. Gephyrin Regulates the Cell Surface Dynamics of Synaptic GABAA Receptors. *J. Neurosci.* **25**, 10469–10478 (2005).
33. Tretter, V. *et al.* The Clustering of GABAA Receptor Subtypes at Inhibitory Synapses is Facilitated via the Direct Binding of Receptor $\alpha 2$ Subunits to Gephyrin. *J. Neurosci.* **28**, 1356–1365 (2008).
34. Niwa, F. *et al.* Gephyrin-Independent GABAAR Mobility and Clustering during Plasticity. *PLoS ONE* **7**, e36148 (2012).
35. Mukherjee, J. *et al.* The residence time of GABAARs at inhibitory synapses is determined by direct binding of the receptor $\alpha 1$ subunit to gephyrin. *J. Neurosci. Off. J. Soc. Neurosci.* **31**, 14677–14687 (2011).
36. Maric, H.-M., Mukherjee, J., Tretter, V., Moss, S. J. & Schindelin, H. Gephyrin-mediated γ -Aminobutyric Acid Type A and Glycine Receptor Clustering Relies on a Common Binding Site. *J. Biol. Chem.* **286**, 42105–42114 (2011).
37. Kowalczyk, S. *et al.* Direct binding of GABAA receptor $\beta 2$ and $\beta 3$ subunits to gephyrin. *Eur. J. Neurosci.* **37**, 544–554 (2013).
38. Panzanelli, P. *et al.* Distinct mechanisms regulate GABA_A receptor and gephyrin clustering at perisomatic and axo-axonic synapses on CA1 pyramidal cells: GABA_A receptors in perisomatic synapses. *J. Physiol.* **589**, 4959–4980 (2011).

39. Kirsch, J. & Betz, H. The Postsynaptic Localization of the Glycine Receptor-Associated Protein Gephyrin Is Regulated by the Cytoskeleton. 9
40. Bausen, M., Fuhrmann, J. C., Betz, H. & O'Sullivan, G. A. The state of the actin cytoskeleton determines its association with gephyrin: Role of ena/VASP family members. *Mol. Cell. Neurosci.* **31**, 376–386 (2006).
41. Flores, C. E. *et al.* Activity-dependent inhibitory synapse remodeling through gephyrin phosphorylation. *Proc. Natl. Acad. Sci.* **112**, E65–E72 (2015).
42. Ghosh, H. *et al.* Several posttranslational modifications act in concert to regulate gephyrin scaffolding and GABAergic transmission. *Nat. Commun.* **7**, (2016).
43. Nguyen, Q.-A., Horn, M. E. & Nicoll, R. A. Distinct roles for extracellular and intracellular domains in neuroligin function at inhibitory synapses. *eLife* **5**,
44. Knuesel, I. *et al.* Altered synaptic clustering of GABAA receptors in mice lacking dystrophin (mdx mice). *Eur. J. Neurosci.* **11**, 4457–4462 (1999).
45. Papadopoulos, T. & Soykan, T. The Role of Collybistin in Gephyrin Clustering at Inhibitory Synapses: Facts and Open Questions. *Front. Cell. Neurosci.* **5**, (2011).
46. Wang, H. & Olsen, R. W. Binding of the GABAA Receptor-Associated Protein (GABARAP) to Microtubules and Microfilaments Suggests Involvement of the Cytoskeleton in GABARAPGABAA Receptor Interaction. *J. Neurochem.* **75**, 644–655 (2002).
47. Hinkle, D. J. & Macdonald, R. L. $\alpha 1$ and $\alpha 2$ GABAA Receptor Currents. 13
48. Connolly, C. N. *et al.* DEPENDENCE ON PROTEIN KINASE C ACTIVITY AND SUBUNIT COMPOSITION. 9

49. Lu, Y. M., Mansuy, I. M., Kandel, E. R. & Roder, J. Calcineurin-Mediated LTD of GABAergic Inhibition Underlies the Increased Excitability of CA1 Neurons Associated with LTP. *Neuron* **26**, 197–205 (2000).
50. Wang, J. *et al.* Interaction of Calcineurin and Type-A GABA Receptor $\alpha 2$ Subunits Produces Long-Term Depression at CA1 Inhibitory Synapses. 11
51. Kittler, J. T. *et al.* Constitutive Endocytosis of GABAA Receptors by an Association with the Adaptin AP2 Complex Modulates Inhibitory Synaptic Currents in Hippocampal Neurons. 6
52. Kittler, J. T. *et al.* Regulation of synaptic inhibition by phospho-dependent binding of the AP2 complex to a YECL motif in the GABAA receptor 2 subunit. *Proc. Natl. Acad. Sci.* **105**, 3616–3621 (2008).
53. Houston, C. M., He, Q. & Smart, T. G. CaMKII phosphorylation of the GABAA receptor: receptor subtype- and synapse-specific modulation. *J. Physiol.* **587**, 2115–2125 (2009).
54. Petrini, E. M. *et al.* Synaptic recruitment of gephyrin regulates surface GABAA receptor dynamics for the expression of inhibitory LTP. *Nat. Commun.* **5**, (2014).
55. Marsden, K. C., Shemesh, A., Bayer, K. U. & Carroll, R. C. Selective translocation of Ca²⁺/calmodulin protein kinase II α (CaMKII α) to inhibitory synapses. *Proc. Natl. Acad. Sci. U. S. A.* **107**, 20559–20564 (2010).
56. Jovanovic, J. N. Brain-Derived Neurotrophic Factor Modulates Fast Synaptic Inhibition by Regulating GABAA Receptor Phosphorylation, Activity, and Cell-Surface Stability. *J. Neurosci.* **24**, 522–530 (2004).

57. Saliba, R. S., Kretschmannova, K. & Moss, S. J. Activity-dependent phosphorylation of GABA_A receptors regulates receptor insertion and tonic current: Activity-dependent phosphorylation of GABA_A receptors. *EMBO J.* **31**, 2937–2951 (2012).
58. Yonemura, S. ERM activation mechanism. 12
59. OTIS, T. S. Lasting potentiation of inhibition is associated with an increased number of γ -aminobutyric acid type A receptors activated during miniature inhibitory postsynaptic currents. 5
60. Kurotani, T., Yamada, K., Yoshimura, Y., Crair, M. C. & Komatsu, Y. State-Dependent Bidirectional Modification of Somatic Inhibition in Neocortical Pyramidal Cells. *Neuron* **57**, 905–916 (2008).
61. Hayashi, Y. Driving AMPA Receptors into Synapses by LTP and CaMKII: Requirement for GluR1 and PDZ Domain Interaction. *Science* **287**, 2262–2267 (2000).
62. Lee, S.-J. R., Escobedo-Lozoya, Y., Szatmari, E. M. & Yasuda, R. Activation of CaMKII in single dendritic spines during long-term potentiation. *Nature* **458**, 299–304 (2009).
63. Kawaguchi, S. -y. & Hirano, T. Sustained Structural Change of GABA_A Receptor-Associated Protein Underlies Long-Term Potentiation at Inhibitory Synapses on a Cerebellar Purkinje Neuron. *J. Neurosci.* **27**, 6788–6799 (2007).
64. Muir, J. *et al.* NMDA receptors regulate GABA_A receptor lateral mobility and clustering at inhibitory synapses through serine 327 on the γ 2 subunit. 6
65. Nahmani, M. & Turrigiano, G. G. Deprivation-Induced Strengthening of Presynaptic and Postsynaptic Inhibitory Transmission in Layer 4 of Visual Cortex during the Critical Period. *J. Neurosci.* **34**, 2571–2582 (2014).

66. Tyagarajan, S. K. & Fritschy, J.-M. GABAA receptors, gephyrin and homeostatic synaptic plasticity. *J. Physiol.* **588**, 101–106 (2010).
67. Marsden, K. C., Beattie, J. B., Friedenthal, J. & Carroll, R. C. NMDA Receptor Activation Potentiates Inhibitory Transmission through GABA Receptor-Associated Protein-Dependent Exocytosis of GABAA Receptors. *J. Neurosci.* **27**, 14326–14337 (2007).
68. Saliba, R. S., Michels, G., Jacob, T. C., Pangalos, M. N. & Moss, S. J. Activity-Dependent Ubiquitination of GABAA Receptors Regulates Their Accumulation at Synaptic Sites. *J. Neurosci.* **27**, 13341–13351 (2007).
69. Smith, K. R. *et al.* Stabilization of GABAA Receptors at Endocytic Zones Is Mediated by an AP2 Binding Motif within the GABAA Receptor 3 Subunit. *J. Neurosci.* **32**, 2485–2498 (2012).
70. Kneussel, M. & Hausrat, T. J. Postsynaptic Neurotransmitter Receptor Reserve Pools for Synaptic Potentiation. *Trends Neurosci.* **39**, 170–182 (2016).
71. Villa, K. L. *et al.* Inhibitory Synapses Are Repeatedly Assembled and Removed at Persistent Sites In Vivo. *Neuron* **89**, 756–769 (2016).
72. Alcor, D., Gouzer, G. & Triller, A. Single-particle tracking methods for the study of membrane receptors dynamics. *Eur. J. Neurosci.* **30**, 987–997 (2009).
73. Saxton, M. J. & Jacobson, K. SINGLE-PARTICLE TRACKING: Applications to Membrane Dynamics. *Annu. Rev. Biophys. Biomol. Struct.* **26**, 373–399 (1997).
74. Bannai, H. *et al.* Bidirectional Control of Synaptic GABAAR Clustering by Glutamate and Calcium. *Cell Rep.* **13**, 2768–2780 (2015).
75. Renner, M., Schweizer, C., Bannai, H., Triller, A. & Lévi, S. Diffusion Barriers Constrain Receptors at Synapses. *PLoS ONE* **7**, e43032 (2012).

76. Masson, J.-B. *et al.* Mapping the Energy and Diffusion Landscapes of Membrane Proteins at the Cell Surface Using High-Density Single-Molecule Imaging and Bayesian Inference: Application to the Multiscale Dynamics of Glycine Receptors in the Neuronal Membrane. *Biophys. J.* **106**, 74–83 (2014).
77. Kusumi, A. *et al.* Paradigm Shift of the Plasma Membrane Concept from the Two-Dimensional Continuum Fluid to the Partitioned Fluid: High-Speed Single-Molecule Tracking of Membrane Molecules. *Annu. Rev. Biophys. Biomol. Struct.* **34**, 351–378 (2005).
78. Bats, C., Groc, L. & Choquet, D. The Interaction between Stargazin and PSD-95 Regulates AMPA Receptor Surface Trafficking. *Neuron* **53**, 719–734 (2007).
79. Kramer, R. H., Mouroto, A. & Adesnik, H. Optogenetic pharmacology for control of native neuronal signaling proteins. *Nat. Neurosci.* **16**, 816–823 (2013).
80. Yizhar, O., Fenno, L. E., Davidson, T. J., Mogri, M. & Deisseroth, K. Optogenetics in Neural Systems. *Neuron* **71**, 9–34 (2011).
81. Rudolph, U. & Knoflach, F. Beyond classical benzodiazepines: Novel therapeutic potential of GABAA receptor subtypes. *Nat. Rev. Drug Discov.* **10**, 685–697 (2011).
82. Jones-Davis, D. M. & Macdonald, R. L. GABAA receptor function and pharmacology in epilepsy and status epilepticus. *Curr. Opin. Pharmacol.* **3**, 12–18 (2003).
83. Möhler, H. GABAA receptor diversity and pharmacology. *Cell Tissue Res.* **326**, 505–516 (2006).
84. Brünig, I., Scotti, E., Sidler, C. & Fritschy, J.-M. Intact sorting, targeting, and clustering of γ -aminobutyric acid A receptor subtypes in hippocampal neurons in vitro: Subcellular Targeting of Gaba_A Receptors. *J. Comp. Neurol.* **443**, 43–55 (2002).

85. Vu, T. Q. *et al.* Activation of membrane receptors by a neurotransmitter conjugate designed for surface attachment. *Biomaterials* **26**, 1895–1903 (2005).
86. Cavalla, D. & Neff, N. H. Photoaffinity Labeling of the GABAA Receptor with [3H]Muscimol. *J. Neurochem.* **44**, 916–921 (1985).
87. Kloda, J. H. & Czajkowski, C. Agonist-, Antagonist-, and Benzodiazepine-Induced Structural Changes in the 1 Met113-Leu132 Region of the GABAA Receptor. *Mol. Pharmacol.* **71**, 483–493 (2006).
88. Sancar, F. & Czajkowski, C. Allosteric modulators induce distinct movements at the GABA-binding site interface of the GABA-A receptor. *Neuropharmacology* **60**, 520–528 (2011).
89. Tochitsky, I. *et al.* Optochemical control of genetically engineered neuronal nicotinic acetylcholine receptors. *Nat. Chem.* **4**, 105–111 (2012).
90. Miller, P. S. & Smart, T. G. Binding, activation and modulation of Cys-loop receptors. *Trends Pharmacol. Sci.* **31**, 161–174 (2010).
91. Padgett, C. L., Hanek, A. P., Lester, H. A., Dougherty, D. A. & Lummis, S. C. R. Unnatural Amino Acid Mutagenesis of the GABAA Receptor Binding Site Residues Reveals a Novel Cation- π Interaction between GABA and β 2Tyr97. *J. Neurosci. Off. J. Soc. Neurosci.* **27**, 886–892 (2007).
92. Nishimura, N. *et al.* Thermal Cis-to-Trans Isomerization of Substituted Azobenzenes II. Substituent and Solvent Effects. *Bull. Chem. Soc. Jpn. - BULL CHEM SOC JPN* **49**, 1381–1387 (1976).

93. Goldstein, P. A. *et al.* Prolongation of Hippocampal Miniature Inhibitory Postsynaptic Currents in Mice Lacking the GABA_A Receptor $\alpha 1$ Subunit. *J. Neurophysiol.* **88**, 3208–3217 (2002).
94. Matthews, W. D. & McCafferty, G. P. Anticonvulsant activity of muscimol against seizures induced by impairment of GABA-mediated neurotransmission. *Neuropharmacology* **18**, 885–889 (1979).
95. Gibbs, J. W., Shumate, M. D. & Coulter, D. A. Differential Epilepsy-Associated Alterations in Postsynaptic GABA_A Receptor Function in Dentate Granule and CA1 Neurons. *J. Neurophysiol.* **77**, 1924–1938 (1997).
96. Dingledine, R., Hynes, M. A. & King, G. L. Involvement of N-methyl-D-aspartate receptors in epileptiform bursting in the rat hippocampal slice. *J. Physiol.* **380**, 175–189 (1986).
97. Szobota, S. *et al.* Remote Control of Neuronal Activity with a Light-Gated Glutamate Receptor. *Neuron* **54**, 535–545 (2007).
98. Fortin, D. L. *et al.* Photochemical control of endogenous ion channels and cellular excitability. *Nat. Methods* **5**, 331–338 (2008).
99. Lüscher, B. & Keller, C. A. Regulation of GABA_A receptor trafficking, channel activity, and functional plasticity of inhibitory synapses. *Pharmacol. Ther.* **102**, 195–221 (2004).
100. Luscher, B., Fuchs, T. & Kilpatrick, C. L. GABA_A Receptor Trafficking-Mediated Plasticity of Inhibitory Synapses. *Neuron* **70**, 385–409 (2011).
101. Maffei, A. *et al.* Emerging Mechanisms Underlying Dynamics of GABAergic Synapses. *J. Neurosci.* **37**, 10792–10799 (2017).

102. de Luca, E. *et al.* Inter-Synaptic Lateral Diffusion of GABA_A Receptors Shapes Inhibitory Synaptic Currents. *Neuron* **95**, 63-69.e5 (2017).
103. Staras, K., Mikulincer, D. & Gitler, D. Monitoring and quantifying dynamic physiological processes in live neurons using fluorescence recovery after photobleaching. *J. Neurochem.* **126**, 213–222 (2013).
104. Lin, W.-C. *et al.* Engineering a Light-Regulated GABA_A Receptor for Optical Control of Neural Inhibition. *ACS Chem. Biol.* **9**, 1414–1419 (2014).
105. Wei, J., Zhang, M., Zhu, Y. & Wang, J.-H. Ca²⁺-calmodulin signalling pathway up-regulates GABA synaptic transmission through cytoskeleton-mediated mechanisms. *Neuroscience* **127**, 637–647 (2004).
106. Meyer, D. K. *et al.* Regulation of Somatodendritic GABA_A Receptor Channels in Rat Hippocampal Neurons: Evidence for a Role of the Small GTPase Rac. **9**
107. Allison, D. W., Gelfand, V. I., Spector, I. & Craig, A. M. Role of Actin in Anchoring Postsynaptic Receptors in Cultured Hippocampal Neurons: Differential Attachment of NMDA versus AMPA Receptors. **14**
108. Gross, G. G. *et al.* An E3-ligase-based method for ablating inhibitory synapses. *Nat. Methods* **13**, 673–678 (2016).
109. Petrini, E. M., Zacchi, P., Barberis, A., Mozrzymas, J. W. & Cherubini, E. Declusterization of GABA_A Receptors Affects the Kinetic Properties of GABAergic Currents in Cultured Hippocampal Neurons. *J. Biol. Chem.* **278**, 16271–16279 (2003).
110. Petrini, E. M., Marchionni, I., Zacchi, P., Sieghart, W. & Cherubini, E. Clustering of Extrasynaptic GABA_A Receptors Modulates Tonic Inhibition in Cultured Hippocampal Neurons. *J. Biol. Chem.* **279**, 45833–45843 (2004).

111. Ali, A. B. & Thomson, A. M. Synaptic γ Subunit-Containing GABA_A Receptors Mediate IPSPs Elicited by Dendrite-Preferring Cells in Rat Neocortex. *Cereb. Cortex* **18**, 1260–1271 (2008).
112. Vargas-Caballero, M., Martin, L. J., Salter, M. W., Orser, B. A. & Paulsen, O. α 5 Subunit-containing GABA_A receptors mediate a slowly decaying inhibitory synaptic current in CA1 pyramidal neurons following Schaffer collateral activation. *Neuropharmacology* **58**, 668–675 (2010).
113. Caraiscos, V. B. *et al.* Tonic inhibition in mouse hippocampal CA1 pyramidal neurons is mediated by γ subunit-containing -aminobutyric acid type A receptors. *Proc. Natl. Acad. Sci.* **101**, 3662–3667 (2004).
114. Prenosil, G. A. *et al.* Specific Subtypes of GABA_A Receptors Mediate Phasic and Tonic Forms of Inhibition in Hippocampal Pyramidal Neurons. *J. Neurophysiol.* **96**, 846–857 (2006).
115. Owen, D. M., Williamson, D., Rentero, C. & Gaus, K. Quantitative Microscopy: Protein Dynamics and Membrane Organisation. *Traffic* **10**, 962–971 (2009).
116. Megías, M., Emri, Z., Freund, T. . & Gulyás, A. . Total number and distribution of inhibitory and excitatory synapses on hippocampal CA1 pyramidal cells. *Neuroscience* **102**, 527–540 (2001).
117. Nusser, Z., Cull-Candy, S. & Farrant, M. Differences in Synaptic GABA_A Receptor Number Underlie Variation in GABA Mini Amplitude. *Neuron* **19**, 697–709 (1997).
118. Nusser, Z. *et al.* Immunocytochemical Localization of the α 1 and β 2/3 Subunits of the GABA_A Receptor in Relation to Specific GABAergic Synapses in the Dentate Gyrus. *Eur. J. Neurosci.* **7**, 630–646 (1995).

119. Murnick, J. G., Dubé, G., Krupa, B. & Liu, G. High-resolution iontophoresis for single-synapse stimulation. *J. Neurosci. Methods* **116**, 65–75 (2002).
120. Müller, C. & Remy, S. Fast Micro-iontophoresis of Glutamate and GABA: A Useful Tool to Investigate Synaptic Integration. *J. Vis. Exp.* (2013). doi:10.3791/50701
121. Richers, M. T., Amatrudo, J. M., Olson, J. P. & Ellis-Davies, G. C. R. Cloaked caged compounds - chemical probes for two-photon optoneurobiology. *Angew. Chem. Int. Ed Engl.* **56**, 193–197 (2017).
122. Kneussel, M. *et al.* Gephyrin-Independent Clustering of Postsynaptic GABA_A Receptor Subtypes. *Mol. Cell. Neurosci.* **17**, 973–982 (2001).
123. NUSSER, Z., SIEGHART, W., BENKE, D., FRITSCHY, J.-M. & SOMOGYI, P. Differential synaptic localization of two major γ -aminobutyric acid type A receptor subunits on hippocampal pyramidal cells. **6**
124. Fritschy, J.-M., Johnson, D. K., Mohler, H. & Rudolph, U. Independent assembly and subcellular targeting of GABA_A-receptor subtypes demonstrated in mouse hippocampal and olfactory neurons in vivo. *Neurosci. Lett.* **249**, 99–102 (1998).
125. Loup, F. *et al.* A Highly Sensitive Immunofluorescence Procedure for Analyzing the Subcellular Distribution of GABA_A Receptor Subunits in the Human Brain. *J. Histochem. Cytochem.* **46**, 1129–1139 (1998).
126. Gerrow, K. & Triller, A. GABA_A receptor subunit composition and competition at synapses are tuned by GABA_B receptor activity. *Mol. Cell. Neurosci.* **60**, 97–107 (2014).
127. Levi, S. Gephyrin Is Critical for Glycine Receptor Clustering But Not for the Formation of Functional GABAergic Synapses in Hippocampal Neurons. *J. Neurosci.* **24**, 207–217 (2004).

128. Kneussel, M. *et al.* Loss of Postsynaptic GABAA Receptor Clustering in Gephyrin-Deficient Mice. 9
129. Connolly, C. N., Krishek, B. J., McDonald, B. J., Smart, T. G. & Moss, S. J. Assembly and cell surface expression of heteromeric and homomeric-aminobutyric acid type A receptors. *J. Biol. Chem.* **271**, 89–96 (1996).
130. Kügler, S., Kilic, E. & Bähr, M. Human synapsin 1 gene promoter confers highly neuron-specific long-term transgene expression from an adenoviral vector in the adult rat brain depending on the transduced area. *Gene Ther.* **10**, 337–347 (2003).